# HADRON SPECTRUM
# AND INFRARED-FINITE BEHAVIOR
# OF QCD RUNNING COUPLING

*G. Ganbold*[*]

Joint Institute for Nuclear Research, Dubna

Institute of Physics and Technology, Ulaanbaatar, Mongolia

[*]E-mail: ganbold@theor.jinr.ru

# HADRON SPECTRUM
# AND INFRARED-FINITE BEHAVIOR
# OF QCD RUNNING COUPLING

## *G. Ganbold*[*]

Joint Institute for Nuclear Research, Dubna

Institute of Physics and Technology, Ulaanbaatar, Mongolia

We study the behavior of the QCD effective coupling $\alpha_s$ in the low-energy region by exploiting the conventional meson spectrum within a relativistic quantum-field model based on analytical confinement of quarks and gluons. The spectra of quark–antiquark and two-gluon bound states are defined by using a master equation similar to the ladder Bethe–Salpeter equation. A new, independent and specific infrared-finite behavior of QCD coupling is found below energy scale $\sim 1$ GeV. Particularly, an infrared-fixed point is extracted at $\alpha_s(0) \simeq 0.757$ for confinement scale $\Lambda = 345$ MeV. We provide a new analytic estimate of the lowest-state glueball mass. As applications, we also estimate masses of some intermediate and heavy mesons as well as the weak-decay constants of light mesons. By introducing only a minimal set of parameters (the quark masses $m_f$ and $\Lambda$) we obtain results in reasonable agreement with recent experimental data in a wide range of energy scale $\sim 0.1$–$10$ GeV. We demonstrate that global properties of some low-energy phenomena may be explained reasonably in the framework of a simple relativistic quantum-field model if one guesses correct symmetry structure of the quark–gluon interaction in the confinement region and uses simple forms of propagators in the hadronization regime. The model may serve as a reasonable framework to describe simultaneously different sectors in low-energy particle physics.

Исследовано поведение эффективной связи КХД $\alpha_s$ в области низкой энергии с помощью спектра мезонов основного состояния в рамках релятивистской квантово-полевой модели с аналитическим конфайнментом кварков и глюонов. Спектры кварк-антикварковых и двухглюонных связанных состояний определяются с помощью главного уравнения, похожего на лестничное приближение Бете–Солпитера. Найдено новое, независимое и специфическое инфракрасно-конечное поведение эффективной связи КХД в области энергии ниже 1 ГэВ. Извлечена, в частности, инфракрасно-фиксированная точка $\alpha_s(0) \simeq 0,757$ при значении шкалы конфайнмента $\Lambda = 345$ МэВ. Получена новая, независимая и аналитическая оценка массы низшего состояния глюбола. В качестве приложения вычислены также массы некоторых промежуточных и тяжелых мезонов и постоянные слабых распадов легких мезонов. С минимальным набором параметров модели (массы кварков $m_f$ и $\Lambda$) получены численные результаты, которые находятся в разумном согласии с экспериментальными данными в широком диапазоне энергии $\sim 0,1$–$10$ ГэВ. Показано, что глобальные свойства некоторых низкоэнергетических феноменов могут быть объяснены разумно в рамках простой релятивистской квантово-полевой модели, если корректно учесть структуру симметрии кварк-глюонного взаимодействия в области конфайнмента и

---

[*]E-mail: ganbold@theor.jinr.ru

использовать простые формы пропагаторов в режиме адронизации. Предложенная модель может служить приемлемой основой для одновременного описания различных областей низкоэнергетической физики частиц.

PACS: 11.10.St; 11.10.Lm; 11.15.Tk; 12.31Mk; 12.38.Aw; 12.38.Qk; 12.39Ki; 12.39.-x; 12.40.Yx; 14.40.-n

## INTRODUCTION

At the present time, QCD is commonly regarded as true theory of strong interactions describing all processes in the hadron world [1]. Confinement and dynamical symmetry breaking are two crucial features of QCD, although they correspond to different energy scales [2, 3]. Confinement is an explanation of the physics phenomenon that color charged particles are not observed; the quarks are confined with other quarks by the strong interaction to form bound states so that the net color is neutral. However, there is no analytic proof that QCD should be color confining and the reasons for quark confinement may be somewhat complicated. There exist different suggestions about the origin of confinement, some dating back to the early 1980s (e.g., [4, 5]) and some more recent based on the Wilson loop techniques [6], string theory quantized in higher dimensions [7], and lattice Monte Carlo simulations (e.g., [8]), etc. It may be supposed that the confinement is not obligatory connected with the strong-coupling regime, but it may be induced by the nontrivial background fields. One of the earliest suggestions in this direction is the *analytic confinement* (AC) based on the assumption that the QCD vacuum is realized by the self-dual vacuum gluon fields which are stable versus local quantum fluctuations and related to the confinement and chiral symmetry breaking [4]. This vacuum gluon field could serve as the true minimum of the QCD effective potential [9]. Particularly, it has been shown that the vacuum of the quark–gluon system has the minimum at the nonzero self-dual homogenous background field with constant strength, and the quark and gluon propagators in the background gluon field represent entire analytic functions on the complex momentum plan $p^2$ [10]. However, direct use of these propagators for low-energy particle physics problems encounters complex formulae and cumbersome calculations. Thus, the self-dual homogeneous gluon field leading to the AC can be considered a good candidate to realize the QCD vacuum. One can say that existing models with AC describe satisfactorily the experimental evidence.

Nowadays, the study of QCD behavior at large distances is an active field of research in particle physics because many interesting and novel behavior is expected in the infrared (IR) region at low energies below 1–2 GeV [11, 12]. Understanding of a number of phenomena such as quark confinement, hadronization

processes, the QCD effective coupling, and nonvanishing vacuum expectation values, etc., requires a correct description of hadron dynamics in the IR domain. However, we are far from understanding how QCD works at longer distances. Being a nonlinear theory with local color gauge symmetry, QCD is quite complicated from the computational point of view, and the conventional methods of calculations require great efforts in making additional assumptions and ideas. In contrast to QED, simple and reliable methods of calculations are still missing in QCD. The well-established conventional perturbation theory cannot be used effectively in the IR region and it is required either to supply with some additional phenomenological parameters (e.g., «effective masses», anomalous vacuum averages, etc.), or to use some nonperturbative methods.

Different nonperturbative approaches have been proposed to deal with the long distance properties of QCD, such as chiral perturbation theory [13], QCD sum rule [14], heavy quark effective theory [15], lattice simulations [16], power correction [17], string-fragmentation [18], Schwinger–Dyson equations, etc. Along outstanding advantages, these approaches have obvious shortcomings. Particularly, rigorous lattice QCD simulations [19] suffer from lattice artifacts and uncertainties and cannot yet give a reliable result in the low-energy hadronization region. The coupled Schwinger–Dyson equation is a continuum method without IR and ultraviolet cutoffs and describes successfully the QCD vacuum and the long distance properties of strong interactions such as confinement and chiral symmetry breaking (e.g., [20]). However, an infinite series of equations requires to make truncations which are gauge-dependent.

Nowadays, the calculations of hadron mass characteristics on the level of experimental data precision still remain among the unsolved problems in QCD due to some technical and conceptual difficulties related with the color confinement and spontaneous chiral symmetry breaking. In such a case, it is useful to investigate the corresponding low-energy effective theories instead of tackling the fundamental theory itself. Although lattice gauge theories are the way to describe effects in the strong-coupling regime, other methods can be applied for some problems not yet feasible with lattice techniques. So data interpretations and calculations of hadron characteristics are frequently carried out with the help of phenomenological models. One of the effective and important tools for studying the relativistic two-particle bound state problem in a field-theory framework is the *Bethe–Salpeter Equation* (BSE) method [21]. The BS amplitude in Minkowski space is singular, and therefore, it is usually solved in Euclidean space to find the binding energy. The solution of the BSE allows one to obtain useful information about the under-structure of the hadrons and thus serves as a powerful test for the quark theory of the mesons. Numerical calculations indicate that the ladder BSE with phenomenological potential models can give satisfactory results (for a review, see [22]) in the IR domain. Moreover, there exist phenomenological indications in fa-

vor of a smooth transition from short distance to long distance physics (see, e.g., [17]).

Therefore, it represents a certain interest to investigate some low-energy physics problems, such as hadronization, glueball states, QCD effective (running) charge, etc., by combining the conception of the AC and the BSE method within simple relativistic models based on physically transparent hypotheses, which can be treated by simple analytic methods.

In the present paper we study the behavior of the QCD running coupling $\alpha_s$ in the low-energy region by exploiting the conventional meson spectrum within a relativistic quantum-field model based on AC of quarks and gluons. The ladder BSE is solved for the spectra of two-quark and two-gluon bound states. A new, independent and specific IR-finite behavior of QCD coupling is found below energy scale $\sim 1$ GeV. We provide also a new analytic estimate of the lowest-state glueball mass. As an application, we estimate masses of some intermediate and heavy mesons as well as the weak decay constants of light mesons. By introducing only a minimal set of parameters (the quark masses $m_f$ and $\Lambda$), we obtain results in reasonable agreement with recent experimental data in a wide range of energy scale $\sim 0.1$–$10$ GeV. The model may serve as a reasonable framework to describe simultaneously different sectors in low-energy particle physics.

In doing so, first, we demonstrate that a simple model of interacting scalar «quarks» and «gluons» provided with an AC can explain qualitatively the physical evidences: free «quarks» and «gluons» are confined, but they may couple into observable bound states, the Regge trajectories of these «hadronic» excitations are asymptotically linear and massless «gluons» may form massive bound states. Then, we take into account the spin, flavor, and color degrees of freedom, and investigate the basic dynamic properties of two-particle bound states of quarks and gluons as well as the QCD effective (running) coupling within relativistic quantum-field models based on AC. For the spectra of two-gluon and quark–antiquark bound states we solve the ladder BSE. The conventional meson masses and the weak decay constants are estimated to extend the consideration. By using a minimal set of model parameters (the quark masses, the coupling constant, and the AC scale) we obtain numerical results which are in reasonable agreement with experimental evidence in the wide range of energy scale from pion mass up to 9.6 GeV. We provide a new, independent, and analytic estimate of the lowest glueball mass, and found it at 1661 MeV. Moreover, we estimate the QCD effective charge $\alpha_s$ in the low-energy region by exploiting the conventional meson spectrum. We also found a new, independent and specific infrared-finite behavior of QCD coupling below energy scale 1 GeV. Particularly, an infrared-fixed point is extracted at $\alpha_s(0) \simeq 0.757$ for confinement scale $\Lambda = 345$ MeV. The model serves as a reasonable framework to describe simultaneously different sectors in low-energy particle physics.

## 1. CONFINEMENT, HADRONIZATION AND GREEN FUNCTIONS

First of all, we would like to clarify the role of the AC in properties of hadrons, the bound states of quarks and gluons by considering a simple relativistic quantum field model. Particularly, we explain qualitatively and semiquantitatively the basic features of experimentally observed meson spectra analyzed in [23].

The hadron spectroscopy as the theory of bound states of quarks, and the phenomenology of the *Regge Trajectories* (RTs) are important and interdependent subjects of investigation in particle physics (see, e.g., [24–26]). The basic characteristics of mesons considered as bound states of quarks and gluons (in contrast to the relations of the $SU_3$ flavor symmetry) can be roughly listed as follows:

— Quarks and gluons are confined (nonobservable).

— Glueballs are bound states of massless gluons and completely relativistic systems.

— The RTs of different families of mesonic orbital excitations are asymptotically linear and their slopes differ insignificantly. Therefore, the slope of RTs may be a universal parameter dictated by the general nature of quark–gluon interaction.

Obviously, these characteristics are hardly obtained in the framework of any local quantum field theory, where the constituent particles, the quarks and gluons are described by the standard Dirac and Klein–Gordon equations. From common point of view, the confinement plays the main role in understanding and explaining this picture. The problem is how to realize mathematically the conception of confinement within a specific theoretical formalism?

The standard QCD calculations leading to linear RTs of hadrons are based on: i) a nonlinear QCD gluon dynamics with a particular infrared behavior of the gluon propagator and ii) a three-dimensional reduction of the relativistic BSE. This results in a linear increasing potential between quarks in three-dimensional space (see, e.g., [27]). This infrared singular behavior is commonly interpreted as quark confinement.

In reality, the modern picture is more complicated (see, for example, [28,29]), but we do not discuss the details here. Note only, it is necessary to overcome some mathematical problems caused by the singularity of the gluon kernel and an ambiguously defined choice of particular reduction of the relativistic two-body BSE (see, e.g., [30]).

In the present paper we show that there exists another possible mechanism explaining the above-mentioned characteristics of meson spectrum, particularly, the properties of RTs. In doing so, we use a simple relativistic quantum-field model of two scalar particles (the prototypes of constituent «quarks» and intermediate «gluons») with the AC. Our approach is based on the following assumptions:

— The AC takes place.

— The interaction is described by a Yukawa-type Lagrangian.

— The coupling constant binding the «quarks» with «gluons» is small.

— Final bound «hadron» states of «quarks» are described by the relativistic ladder BSE without using any 3D-reduction.

In addition we demonstrate a mathematical sketch of calculations of two-body bound-state spectrum within the BSE in the weak-coupling regime. In doing so, we use simple relativistic models based on physically transparent hypotheses, which can be treated by simple analytic methods. We believe that the AC is the basic underlying principle leading to a qualitatively correct description of main characteristics of meson spectra. In any case our models represent certain theoretical interest because they clarify the underlying physical principles of the meson spectrum.

**1.1. Analytic Confinement.**   In particle physics there exist several models based on the idea of AC. According to Leutwyler [4], this gluon configuration is stable over local quantum fluctuations, and can lead to the quark and gluon confinement as well as a necessary chiral symmetry breaking. Hereby, propagators of quarks and gluons in this field are entire analytic functions in the $p^2$-complex plane, i.e., the AC takes place. An approach, based on the assumption that QCD vacuum is realized by the self-dual homogeneous vacuum gluon field which is the classical solution of the Yang–Mills equations, was developed in [10, 31]. This approach contains a minimal set of parameters: the gauge coupling constant, the strength of the vacuum field and the quark masses. The Quark Confinement Model [32] treats light hadrons as collective colorless excitations of quark–gluon interactions while the analytic quark confinement is provided by averaging over gluon backgrounds. The analytic form of the form factor providing the quark confinement is a phenomenological function unique for all processes in the low-energy physics. This model reproduces the low-energy relations of chiral theory in the case of zero momentum and allows one to obtain more sophisticated hadron characteristics such as slope parameters and form factors.

Generally, one may expect that a theoretical description of colorless hadrons considered as bound states of quarks and gluons, when the confinement is taken into account and an averaging over all nonobservable color degrees of freedom is performed, can lead to a physical picture, where the quarks and gluons are realized in the form of some phenomenological «bricks». We suppose that a successful guess of the structure of these «bricks» in the confinement region can result, particularly, in a qualitatively correct description of the basic features of the meson spectrum. Our guess is that the AC realizes these «bricks».

However, real calculations of different amplitudes in particle physics require to take into account simultaneously the confinement as well as some quantum characteristics associated with color, flavor, and spin within a chiral symmetry breaking. Besides, analytic calculations within these approaches are quite cumbersome. In addition, it is necessary to note that there exists a prejudice to the idea of the AC (see, for example, [33]). Therefore, it seems reasonable to

consider simple quantum field models in order to investigate qualitatively just «pure» effects due to AC.

Particularly, within a quantum-field model, the quark confinement may be explained as the absence of quark poles and thresholds in Green's function. Following this idea, the conception of AC assumes that the QCD vacuum is realized by the self-dual vacuum gluon fields which are stable versus local quantum fluctuations and related to the confinement and chiral symmetry breaking [4]. This vacuum gluon field serves as the true minimum of the QCD effective potential [9]. The vacuum of the quark–gluon system has the minimum at the nonzero self-dual homogenous background field with constant strength. Then, the quark and gluon propagators in the background gluon field represent entire analytic functions in Euclidean space [10]. In previous papers [34, 35] we developed relativistic quantum field models with AC. Similar ideas have been realized in infrared confinement by introducing an IR cutoff within a Nambu–Jona-Lasino model [36, 37].

**1.2. Green Functions in Hadronization Region.** The effective charge is strongly governed by the detailed dynamics of the strong interaction and may depend on some of the most fundamental Green functions of QCD, such as the gluon and quark propagators [38]. Green functions in QCD are tightly connected to confinement and are ingredients for hadron phenomenology. However, any widely accepted and rigorous analytic solutions to these propagators are still missing. One may encounter difficulties by defining the explicit quark and gluon propagator at the confinement scale. Nowadays, IR behaviors of the quark and gluon propagators are not well-established and need to be more specified [39].

From our point of view, any acceptable description of quarks and gluons and their hadronization on large distances, where the confinement of quarks and gluons takes place, directly depends on the structure of QCD vacuum, and this structure is not well established yet. In other words, the propagators of quarks and gluons on large distances are quite far from those given by standard Dirac and Klein–Gordon equations.

The matrix elements of hadron processes at large distance are integrated characteristics of the vertices, quark, and gluon propagators and the solution of the BS equation should not be too sensitive to the details of propagators. Taking into account the correct global symmetry properties and their breaking, also by introducing additional physical parameters, may be more important than the detailed working out of propagators (e.g., [40]). In previous papers we exploited simple forms of quark and gluon propagators [34, 35] which were entire analytic functions in Euclidean space and behaved similar to the explicit propagators dictated by AC [10].

The structure of the QCD vacuum is not well established and one may encounter difficulties by defining the explicit quark and gluon propagator at the confinement scale. Obviously, the conventional Dirac and Klein–Gordon forms

of the propagators cannot adequately describe confined quarks and gluons in the hadronization region. Besides, the currents and vertices used to describe the connection of quarks (and gluons) within hadrons cannot be purely local.

Because of the complexity of explicit Green functions derived in [10], we examine simpler propagators exhibiting similar characteristics.

Following [41] we introduce the quark propagator as follows:

$$\tilde{S}^{ab}_{\pm}(\hat{p}) = \delta^{ab} \frac{i\hat{p} + m_f[1 \pm \gamma_5\ \omega(m_f/\Lambda)]}{\Lambda m_f} \exp\left\{-\frac{p^2 + m_f^2}{2\Lambda^2}\right\}, \qquad (1)$$

where $\hat{p} = p_\mu \gamma_\mu$ and $\omega(z) = (1 + z^2/4)^{-1}$. The sign «$\pm$» in the quark propagator corresponds to the self- and antiself-dual modes of the background gluon fields. Note, the interaction of the quark spin with the background gluon field generates a singular behavior $\tilde{S}_{\pm}(\hat{p}) \sim 1/m_f$ in the massless limit $m_f \to 0$. This corresponds to the zero-mode solution (the lowest Landau level) of the massless Dirac equation in the presence of external gluon background field and generates a nontrivial quark condensate

$$\langle \bar{q}_f(0) q_f(0) \rangle = - \int \frac{d^4 p}{(2\pi)^4} \mathrm{Tr}\left[\tilde{S}_{\pm}(\hat{p})\right] = -\frac{6\Lambda^3}{\pi^2} \exp\left\{-\frac{m_f^2}{2\Lambda^2}\right\} \neq 0$$

indicating the broken chiral symmetry as $m_f \to 0$. A mass splitting appears between vector and pseudoscalar mesons ($M_V > M_P$) consisting of the same quark content.

For the gluon propagator we choose the following form (in Feynman gauge) [35]:

$$\tilde{D}^{AB}_{\mu\nu}(p) = \delta^{AB} \frac{\delta_{\mu\nu}}{p^2} \exp\left(-p^2/4\Lambda^2\right). \qquad (2)$$

Remember, that within the model the quark and gluon propagators $\tilde{S}(\hat{p})$ and $\tilde{D}(p)$ in (33) are entire analytic functions in the Euclidean space.

Both propagators in (1) and (2) are entire analytic functions in Euclidean space and may serve simple and reasonable approximations to the explicit propagators under the AC (see, e.g., [35, 41]).

In the next section we investigate the pure role of the AC in formation of two-particle bound states by omitting quantum degrees of freedom such as the spin, color, and flavor.


## 2. SCALAR «TOY» MODELS WITH ANALYTIC CONFINEMENT

Let us consider a simple system, a Yukawa model of two interacting scalar fields $\Phi(x)$ and $\varphi(x)$ described by the following Lagrangian in the Euclidean

domain:

$$\mathcal{L}(x) = -\Phi^+(x)\,S^{-1}(\Box)\,\Phi(x) - \frac{1}{2}\varphi(x)\,D^{-1}(\Box)\,\varphi(x) - g\Phi^+(x)\,\Phi(x)\,\varphi(x)\,, \quad (3)$$

where coupling constant $g$ is supposed sufficiently small.

We postulate that the AC takes place here. It means that the Fourier transforms of propagators of confined particles $\Phi$ and $\varphi$ are entire analytic functions in the complex $p^2$-plane, so $S^{-1}(p^2)$ and $D^{-1}(p^2)$ have no zero at any finite complex $p^2$. Hence, the equations for the free fields

$$S^{-1}(\Box)\Phi(x) = 0, \quad D^{-1}(\Box)\varphi(x) = 0 \quad (4)$$

result only in the trivial solutions $\Phi(x) \equiv 0$ and $\varphi(x) \equiv 0$. We call this property AC, i.e., the corresponding particles exist only in virtual states [32, 33]. One can say that these fields describe constituent particles, i.e., $\Phi(x)$ and $\varphi(x)$ represent scalar «quarks» and scalar «gluons», respectively.

«Two-quark» bound states can be found in the following way. Let us consider the partition function

$$Z = \int\int\int \delta\Phi\,\delta\Phi^+\delta\phi\,\exp\left[-(\Phi^+S^{-1}\Phi) - \frac{1}{2}(\varphi D^{-1}\varphi) - g(\Phi^+\Phi\varphi)\right]. \quad (5)$$

This partition function is written in the quark and gluon variables. Our aim is to rewrite $Z$ in terms of «hadron» fields in order to realize the so-called *quark–hadron duality*.

Integration over $\varphi$ results in

$$Z = \int\int \delta\Phi\delta\Phi^+ \,\exp\left[-(\Phi^+S^{-1}\Phi) + \frac{g^2}{2}(\Phi^+\Phi D\Phi^+\Phi)\right]. \quad (6)$$

Let us introduce a complete orthonormal system $\{U_Q(y)\}$:

$$\int dy\,U_Q(y)U_{Q'}(y) = \delta_{QQ'}, \quad \sum_Q U_Q(y)U_{Q'}(y') = \delta(y - y'), \quad (7)$$

where $Q = \{n, l, \{\mu\}\}$ is a set of radial $n$, orbital $l$ and magnetic $\{\mu\} = (\mu_1, \ldots, \mu_l)$ quantum numbers. Then, the term $L_2[\Phi] = (\Phi^+\Phi D\Phi^+\Phi)$ can be rewritten

$$L_2[\Phi] = \frac{g^2}{2}\int\int dx_1\,dx_2\,\Phi^+(x_1)\Phi(x_1)D(x_1 - x_2)\Phi^+(x_2)\Phi(x_2) =$$

$$= \frac{g^2}{2}\int dx \int\int dy_1\,dy_2\,\sqrt{D(y_1)}J(x, y_1)\delta(y_1 - y_2)\sqrt{D(y_2)}J^+(x, y_2) =$$

$$= \frac{g^2}{2}\sum_Q \int dx\,J_Q(x)\,J_Q(x), \quad (8)$$

with $x_1 = x + y/2$, $x_2 = x - y/2$ and

$$J(x, y) = \Phi^+ \left( x + \frac{1}{2} y \right) \Phi \left( x - \frac{1}{2} y \right) = \Phi^+(x)\, e^{\frac{y}{2} \overleftrightarrow{\partial}} \Phi(x),$$

$$J^+(x, y) = J(x, -y), \quad J_Q(x) = \Phi^+(x) V_Q(\overleftrightarrow{\partial}) \Phi(x), \tag{9}$$

$$J_Q^+(x) = J_Q(x), \quad V_Q(\overleftrightarrow{\partial}) = i^l \int dy \sqrt{D(y_1)} U_Q(y)\, e^{\frac{y}{2} \overleftrightarrow{\partial}},$$

where $V_Q(\overleftrightarrow{\partial})$ is a nonlocal vertex.

By using the Gaussian functional representation we write

$$e^{L_2[\Phi]} = \exp\left[ \frac{g^2}{2} \sum_Q \int dx\, J_Q(x)\, J_Q(x) \right] =$$

$$= \int \prod_Q \delta B_Q\, \exp\left[ -\frac{1}{2} \sum_Q (B_Q\, B_Q) + g \sum_Q (B_Q\, J_Q) \right].$$

Substituting this representation into (6) and by integrating over $\Phi$ we obtain

$$Z = \int \prod_Q \delta B_Q\, \exp\left\{ -\frac{1}{2} \sum_Q (B_Q\, B_Q) - \text{Tr}\, \ln(1 - g B_Q\, V_Q S) \right\} =$$

$$= \int \prod_Q \delta B_Q\, \exp\left\{ -\frac{1}{2} \sum_{QQ'} (B_Q [\delta_{QQ'} - \alpha \Pi_{QQ'}] B_{Q'}) + W_I[gB] \right\}, \tag{10}$$

where

$$W_I[gB] = -\text{Tr}\left[ \ln\left(1 - g B_Q V_Q S\right) + \frac{g^2}{2} B_Q\, V_Q\, S B_{Q'} V_{Q'} S \right]$$

is a functional describing interactions of fields $B_Q$.

**2.1. The Bethe–Salpeter Kernel.** Polarization kernel $\alpha \Pi_{QQ'}$ in the one-loop approximation reads

$$\alpha \Pi_{QQ'}(z) = \int \int dy_1\, dy_2\, U_Q(y_1) \alpha \Pi(z; y_1, y_2) U_{Q'}(y_2),$$

$$\alpha \Pi(z; y_1, y_2) = g^2 \sqrt{D(y_1)} S\left( z + \frac{y_1 - y_2}{2} \right) S\left( z - \frac{y_1 - y_2}{2} \right) \sqrt{D(y_2)},$$

where $z = x_1 - x_2$ and $\alpha = (g/4\pi\Lambda)^2$. Its Fourier transform reads

$$\alpha \tilde{\Pi}_{QQ'}(p) = \int \int dy_1\, dy_2\, U_Q(y_1) \alpha \tilde{\Pi}_p(y_1, y_2) U_{Q'}(y_2), \tag{11}$$

$$\alpha\tilde{\Pi}_p(y_1, y_2) =$$

$$= g^2 \sqrt{D(y_1)} \int \frac{dk}{(2\pi)^4} \, e^{-ik(y_1-y_2)} \tilde{S}\left(k + \frac{p}{2}\right) \tilde{S}\left(k - \frac{p}{2}\right) \sqrt{D(y_2)}.$$

Suppose, the orthonormal system $\{U_Q(y)\}$ diagonalizes the kernel in (11). It means that we solve the eigenvalue problem

$$\int dy' \alpha\tilde{\Pi}_p(y, y') U_Q(y) = E_Q(-p^2) \, U_Q(y), \tag{12}$$

where $E_Q(-p^2) = E_{nl}(-p^2)$, i.e., the eigenvalues are degenerated over the magnetic quantum numbers $\{\mu\}$. We stress that the Bethe–Salpeter kernel in (12) is real and symmetric, therefore, variational methods can be applied for its further evaluation.

Then, the polarization operator in (11) reads:

$$\alpha\tilde{\Pi}_{QQ'}(p) = E_Q(-p^2)\delta_{QQ'}. \tag{13}$$

Note that diagonalization (13) is nothing else but the solution of the ladder BSE. The standard form of the BSE may be obtained, if one introduces in (12) new functions $U_Q(y) = \sqrt{D(y)}\Psi_Q(y)$ and goes to the momentum space.

By introducing a Gaussian measure defined by

$$G_Q^{-1}(x_1 - x_2) = [1 - E_Q(\square)] \, \delta(x_1 - x_2), \quad p^2 = -\square$$

we rewrite the partition function (10) in the final form

$$Z = \int \prod_Q \delta\tilde{B}_Q \, \exp\left[-\frac{1}{2}\sum_Q (B_Q \, G_Q^{-1} B_Q) + W_I[gB]\right]. \tag{14}$$

We stress that this representation is completely equivalent to the initial one (5). It is a mathematical realization of the quark–hadron duality in the model under consideration. From physical point of view, we pass on from the world containing fields $\Phi$ and $\phi$ to the world of bound states $\{B_Q\}$. The field variables $\{B_Q\}$ can be interpreted as fields of particles with quantum numbers $Q = \{nl\}$ and masses $M_Q$, if the Green function $\tilde{G}_Q(p^2) = \dfrac{1}{1 - E_Q(-p^2)}$ has a simple pole in the Minkowski space $(p^2 = -M_Q^2)$. The masses of two-particle bound states are defined by the equation:

$$1 = E_Q(M_Q^2). \tag{15}$$

Formally, $G_Q^{-1}(-\square)$ defines the kinetic term of the field $B_Q$. To go to its standard form, we expand it in the vicinity of $p^2 = -M_Q^2$ as follows:

$$1 - E_Q(-p^2) = Z_Q(p^2 + M_Q^2) + O[(p^2 + M_Q^2)^2], \quad Z_Q = -E_Q'(-M_Q^2) > 0.$$

The positive constant $Z_Q$ provides the renormalization of the wave function of the field $B_Q$. We rewrite the kinetic and interaction parts in terms of the renormalized fields $\tilde{B}_Q(p) = Z_Q^{-1/2}\tilde{\mathcal{B}}_Q(p)$ as follows:

$$\left(\tilde{B}_Q^+(p)\left[1 - E_Q(-p^2)\right]\tilde{B}_Q(p)\right) =$$
$$= \left(\tilde{\mathcal{B}}_Q^+(p)\left[(p^2 + M_Q^2) + O((p^2 + M_Q^2)^2)\right]\tilde{\mathcal{B}}_Q(p)\right),$$

$$W_I[gB] = W_I[g_{\text{eff}}\mathcal{B}], \quad g_Q^{\text{eff}} = gZ_Q^{-1/2} = \frac{g}{\sqrt{-E_Q'(-M_Q^2)}} > 0. \tag{16}$$

The functional $W_I[g_{\text{eff}}\mathcal{B}]$ describes all «strong interactions» of the «mesons» $\mathcal{B}_Q$. In addition, it should be stressed that the effective coupling constant $g_Q^{\text{eff}}$ in (16), defining the strength of boson interactions does not explicitly depend on the initial coupling constant $g$ because of relation $E_Q'(-M_Q^2) \sim g$.

Below we consider with two specific versions of the AC. Note, both these models realize the «quark» and «gluon» confinement only. Other important quantum characteristics as color, flavor, and spin with an appropriate chiral broken symmetry are not taken into account yet.

**2.2. The Virton Model.** In the first simplest model we consider two massless particles and pure Gaussian exponents for the propagators:

$$S(x_1 - x_2) = S(\square_{x_1})\,\delta(x_1 - x_2) = \frac{\Lambda^2}{(4\pi)^2}\exp\left[-\frac{1}{4}\Lambda^2(x_1 - x_2)^2\right],$$

$$\tilde{S}(p^2) = \frac{1}{\Lambda^2}\exp\left(-\frac{p^2}{\Lambda^2}\right),$$

$$D(x_1 - x_2) = D(\square_{x_1})\delta(x_1 - x_2) = \frac{\Lambda^2}{(4\pi)^2}\exp\left[-\frac{1}{4}\Lambda^2(x_1 - x_2)^2\right], \tag{17}$$

$$\tilde{D}(p^2) = \frac{1}{\Lambda^2}\exp\left(-\frac{p^2}{\Lambda^2}\right),$$

where the only parameter $\Lambda$ represents the scale of confinement. Consequently, $1/\Lambda$ implies the characteristic «radius» of AC. From a physical point of view this model is important because the eigenfunctions and eigenvalues of the relativistic BSE within one-particle exchange approximation can be found explicitly and the

obtained RTs are purely linear. In some sense, this model can be considered a «relativistic oscillator» because the exact solution possesses equidistant spectra resulting in pure linear RTs. We call this case *the Virton Model*.

Due to the pure Gaussian character of the propagators in this model, the polarization kernel (11) becomes quite simple [42]:

$$
\alpha \tilde{\Pi}_p(y, y') = \alpha \left( \frac{\Lambda^2}{8\pi} \right)^2 \exp\left( -\frac{p^2}{2\Lambda^2} \right) K(y, y'),
$$

$$
K(y, y') = \exp\left[ -\frac{\Lambda^2}{4}(y^2 - yy' + y'^2) \right].
\tag{18}
$$

Explicit diagonalization of kernel $K(y, y')$ on $\{U_Q(y)\}$ results in the eigenvalues:

$$
\kappa_Q = \kappa_{nl} = \kappa_0 \left( \frac{1}{2 + \sqrt{3}} \right)^{2n+l}, \quad \kappa_0 = \left( \frac{8\pi}{\Lambda^2(2 + \sqrt{3})} \right)^2.
\tag{19}
$$

Corresponding eigenfunctions $U_Q(y)$ are given in Appendix A.

Therefore, the mass spectrum of two-particle bound states can be found explicitly

$$
M_Q^2 = M_{nl}^2 = 2\Lambda^2 \ln\frac{\alpha_c}{\alpha} + (2n + l)2\Lambda^2 \ln(2 + \sqrt{3}), \quad \alpha_c = \left(2 + \sqrt{3}\right)^2.
\tag{20}
$$

Thus, a pure Gaussian form of AC (17) leads to the linear and parallel RTs. The slope of RTs is defined only by the scale of the confinement region $\Lambda$ and does not depend on $\alpha$ and other dynamic constants. Bound states exist for $\alpha < \alpha_c$. If $\alpha \ll \alpha_c$, the size of the confinement region is remarkably larger than the Compton length of any bound state

$$
r_{\text{conf}} \sim \frac{1}{\Lambda} \gg \frac{1}{M_Q} \sim l_Q.
$$

In other words, all physical particles described by the fields $B_Q(x)$ and all physical transformations involving them take place inside the confinement region.

**2.3. The Scalar Confinement Model.** The second model implies that there exists a certain dynamical mechanism generating AC of standard particles with initial masses $m$ and $0$. So, we introduce the second parameter, a «quark» mass $m$. The propagators are given in more realistic forms [43]:

$$
S(z) = \left( \frac{\Lambda}{4\pi} \right)^2 \int\limits_0^1 \frac{d\alpha}{\alpha^2} \exp\left( -\frac{\alpha m^2}{\Lambda^2} - \frac{\Lambda^2 z^2}{4\alpha} \right),
$$

$$\tilde{S}(p^2) = \frac{1}{p^2 + m^2} \left[ 1 - \exp\left( -\frac{p^2 + m^2}{\Lambda^2} \right) \right],$$

$$D(z) = \frac{1}{(2\pi)^2 x^2} \exp\left( -\frac{\Lambda^2 z^2}{4} \right), \quad \tilde{D}(p^2) = \frac{1}{p^2} \left[ 1 - \exp\left( -\frac{p^2}{\Lambda^2} \right) \right].$$

$$(21)$$

In the deconfinement limit $\Lambda \to 0$ this model allows one to obtain the conventional propagators of massive and massless scalar particles. Within this model we can analyze the influence of the mass parameter $\nu = m/\Lambda$ on the behavior of the meson spectrum. We call this case *the Scalar Confinement Model*. We show that this model describes qualitatively well dynamic characteristics of meson spectra.

In order to solve the eigenvalue problem (12) we will use the variational principle because the kernel $\tilde{\Pi}_p(y, y')$ is real and symmetric. For further simplicity, we consider only the orbital excitations, i.e., $n = 0$ and $Q = \{0, l, \{\mu\}\}$.

According to (15), the mass of the bound state is determined by the following variational equation:

$$1 = \alpha \epsilon_l \left( \frac{M_l}{2\Lambda}, \frac{m}{\Lambda} \right) = \max_{\Psi_Q} \sum_{\{\mu\}} \int \int dy_1 \, dy_2 \, \Psi_Q(y_1) \alpha \Pi_p(y_1, y_2) \Psi_Q(y_2),$$

$$p^2 = -M_l^2.$$

$$(22)$$

Note, the variational optimization gives an upper bound to the mass $M_l^2$ because for $M_l^2 > 0$

$$\alpha \epsilon_l \left( \frac{M_l}{2\Lambda}, \frac{m}{\Lambda} \right) \leqslant E_l(M_l^2).$$

Let us introduce a normalized trial wave function:

$$\Psi_{l\{\mu\}}(x, a) = C_l \, T_{l\{\mu\}}(x) \sqrt{D(x)} \exp\left( -\frac{\Lambda^2}{4} a x^2 \right),$$

$$(23)$$

$$C_l = \Lambda^{l+1} \sqrt{\frac{(1 + 2a)^{l+1}}{2^l (l+1)!}}, \quad \sum_{\{\mu\}} \int dx \, \left| \Psi_{l\{\mu\}}(x, a) \right|^2 = 1,$$

where $a$ is a variational parameter. The four-dimensional spherical orthogonal harmonics $T_{l\{\mu\}}(x)$ are defined in Appendix A. We suppose that the test function in (23) should be a good guess to the exact one because the kernel (11) is proportional to $\sqrt{D(y)}$ and $S(y)$ is of the Gaussian type [42].

Further we use the following relation:

$$\tilde{\Phi}_{l\{\mu\}}(k,a) \equiv i^l \int dx\, e^{-ikx}\sqrt{D(x)}\Psi_{l\{\mu\}}(x,a) =$$

$$= \frac{C_l}{(2\pi)^l}T_{l\{\mu\}}(k)\int d^{4+2l}Y\, e^{-iKY}D(Y)0\, e^{-aY^2},$$

where $K, Y \in \mathbf{R}^{4+2l}$, $k^2 = K^2$ and the rotational symmetry $D(y^2) = D(Y^2)$ has been taken into account. Then, one obtains [43]

$$\sum_{\mu}\tilde{\Phi}_{l\{\mu\}}(k,a)\tilde{\Phi}_{l\{\mu\}}(k,a) = \frac{C_l^2\, k^{2l}(l+1)}{2^{4+3l}}\left[\int_0^{u_0} du\, u^l\, e^{-uk^2/4}\right]^2 = 1,$$

$$u_0 = \frac{4}{\Lambda^2(1+a)}. \tag{24}$$

Substituting (21), (23), and (24) into (22) and after some calculations we arrive at

$$1 = g^2 \max_a \int \frac{dk}{(2\pi)^4}\sum_{\{\mu\}}\tilde{\Phi}_{l\{\mu\}}(k,a)\tilde{S}\left(k+\frac{p}{2}\right)\tilde{S}\left(k-\frac{p}{2}\right)\tilde{\Phi}_{l\{\mu\}}(k,a) =$$

$$= \frac{\alpha}{l!}\max_c\left\{[4c(1-c)]^{l+1}\int_0^1\!\!\int dt\, ds\, e^{(\mathcal{M}_l^2-\nu^2)(t+s)}R_l(t,s,\chi_l)\right\}, \tag{25}$$

where $p = (iM_l, 0, 0, 0)$ and

$$R_l(t,s,\chi_l) = \int_0^1\!\!\int du\, dv\, e^{-\chi_l^2/b}(uw)^l F_l(b,\chi_l),$$

$$F_l(b,\chi_l) = \frac{1}{\pi^2}e^{\chi_l^2/b}\int d^4k\, k^{2l}\, e^{-k^2b-kp(t-s)} = e^{\chi_l^2/b}\left(-\frac{\partial}{\partial b}\right)^l\left[\frac{1}{b^2}e^{-\chi_l^2/b}\right],$$

$$\nu = \frac{m}{\Lambda}, \quad \mathcal{M}_l = \frac{M_l}{2\Lambda}, \quad \chi_l^2 = \mathcal{M}_l^2\,(t-s)^2, \quad b = t+s+2c(u+w).$$

Variational equation (25) defines the relation between parameters $M_l$, $\alpha$, $\nu$, and $l$.

In the deconfinement limit $\Lambda \to 0$ our variational estimation results in a qualitatively correct behavior (for details see Appendix B) of the final bound-state mass

$$M_0 = 2m - \frac{\alpha_0^2}{2}m\, K + O(\alpha_0^4), \quad \alpha_0 = \left(\frac{g}{4\pi m}\right)^2, \quad K = 0.6403\ldots,$$

i.e., we get the standard nonrelativistic (the coupling constant $\alpha_0$ is small) behavior for a bound state under the Coulomb potential.

*2.3.1. The Ground State.*   Let us consider the lowest state with $l = 0$. The equation of the bound state becomes

$$\epsilon_0 \left( \mathcal{M}_0, \nu \right) = \max_c \left\{ 4c(1-c) \int\limits_0^1 \int dt\, ds \int\limits_0^1 \int du\, dv \times \right.$$

$$\left. \times \frac{\exp\left[ -\nu^2(t+s) + \mathcal{M}_0^2 \left( (t+s) - \frac{(t-s)^2}{t+s+2c(u+v)} \right) \right]}{[t+s+2c(u+v)]^2} \right\} = \frac{1}{\alpha}. \quad (26)$$

We have analyzed (26) at different regimes of parameters $\alpha$, $m$, and $\Lambda$ and have solved it numerically for $\mathcal{M}_0$. Some of obtained results are represented in Fig. 1.

By analyzing our results we can conclude the following remarks:

1. There exists a critical coupling constant $\alpha_c = 1.9149\ldots$ obeying the equation

$$\epsilon_0(0,0) = \frac{1}{\alpha_c}. \quad (27)$$

It means that there may exist a bound state with $m = 0$, $M_0 = 0$, i.e., massless «gluons» are able to produce a massless «hadron» bound state.
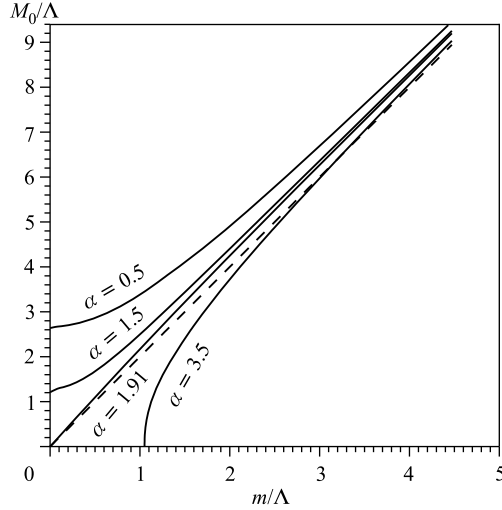


Fig. 1. The mass $\mathcal{M}_0 = M_0/\Lambda$ of the two-particle ground state ($l = 0$) as a function of the mass $\nu = m/\Lambda$ of the «constituent» particle. Dashed line corresponds to the case, when $M_0 = 2m$. The physical picture takes place only for relative weak coupling constant $\alpha < \alpha_c = 1.9149\ldots$

2. If $\alpha \leqslant \alpha_c$, the mass of the «hadron» bound state obeys the inequality $M_0 \geqslant 2m$ for $\forall m \geqslant 0$. Particularly, for $\alpha < \alpha_c$ there exist states with $M_0 > 0$ for $m = 0$, i.e., massless «gluons» can produce massive «hadron» bound states — the «glueballs». For heavy «quarks» ($m \gg \Lambda$) one obtains an asymptotical behavior

$$M_0^2 = 4m^2 + \frac{\Lambda^2}{2} \ln \left( \frac{m}{\Lambda} \right) + O(1). \tag{28}$$

3. If the coupling strength exceeds the critical value $\alpha > \alpha_c$, the physical condition $M_0^2 \geqslant 0$ results in the requirement $m \geqslant m_c$, where

$$\epsilon_0 \left( 0, \frac{m_c}{\Lambda} \right) = \frac{1}{\alpha} < \frac{1}{\alpha_c}. \tag{29}$$

In other words, for a fixed $\alpha > \alpha_c$ the mass of the «quark» should exceed the critical value $m_c$ in order to constitute physically meaningful bound states. Particularly, there exist massless «hadrons» $M_0 = 0$ constituted of two massive «quarks» with $m = m_c$. This kind of «mass annihilation» does not coincide with conventional physical conception.

Thus, we conclude that the value of the coupling constant $\alpha = (g/4\pi\Lambda)^2$ plays a crucial role in formulation of the final two-particle bound states and there exist two physically different pictures:

• If $\alpha < \alpha_c$, there exist physically allowed bound states with masses $M_0 > 2m$. Particularly, glueballs exist as massive bound states of massless constituent particles.

• If $\alpha > \alpha_c$, there exists a critical mass of the constituent particle $m_c$, so that bound states can exist only for $m > m_c$. Therefore, a massless meson as a bound state of two massive quarks can exist. But, any glueballs cannot exist at all because $0 \neq m > m_c$.

Therefore, we can conclude that a physically reasonable picture can be realized within our model only for relatively small coupling constant $\alpha < \alpha_c$.

*2.3.2. Orbital Excitations and Regge Trajectories.* In general case, formula (25) defines the mass of an orbital excitation $M_l$ as a function of input parameters: the coupling constant $\alpha$, the mass of constituent «quark» $m$ and the confinement scale $\Lambda$ at any given orbital quantum number $l$.

As mentioned above, we believe that the Scalar Confinement Model grasps the basic characteristics of meson spectrum, it especially should be effective in describing the orbital excitations which are determined mainly by interactions on large distances, where detailing of the quark–gluon interaction are not so important. Therefore, we are able to evaluate the confinement scale $\Lambda$ and the coupling constant $\alpha$ by applying (25) to a set of experimental data on the RTs. Note, the pion RT is not suitable for our consideration because the lowest $\pi$ meson has

anomalously small mass caused by the mechanism of the broken chiral symmetry, which is absent in the model under consideration. So, we choose the $K$-meson family of orbital excitations $\{K(0.495), K(1.270)/K(1.400), K(1.770)\}$ with $l = \{0, 1, 2\}$. Here and below all masses are given in GeV. Since $K$ mesons consist of $u\,(d)$ and $s$ quarks with different masses $m_u$ and $m_s$, we modify formula (25) as follows:

$$1 = \frac{\alpha}{l!} \max_{c} \left\{ [4c(1-c)]^{l+1} \int\limits_{0}^{1}\!\!\int dt\,ds\, \mathrm{e}^{-(\nu_u^2 t + \nu_s^2 s) + (t+s)\mathcal{M}_l^2} R_l(t, s, \chi_l) \right\},$$

(30)

$$\nu_u = \frac{m_u}{\Lambda}, \quad \nu_s = \frac{m_s}{\Lambda}.$$

Thus, we solve the problem by finding $\alpha$ and $\Lambda$ for given $m_u$ and $m_s$ and $M_l$ by using data on the $K$-meson family. For each member of this family we have obtained the dependence $\Lambda = \Lambda(\alpha)$ at fixed «constituent quark» masses $m_u = 0.010$ and $m_s = 0.100$. The obtained curves $\Lambda = \Lambda(\alpha)$ are plotted in Fig. 2. We see that our input parameters $\alpha$ and $\Lambda$ should be localized in relative short intervals to fit the kaon Regge trajectory, namely

$$\Lambda = 0.4{-}0.5 \text{ GeV}, \qquad \alpha = 1.5{-}1.9. \tag{31}$$

Our preliminary analyses performed for other meson families $(\pi, K^*, \rho)$ indicate that this choice of our fundamental parameters is able to fit satisfactorily the
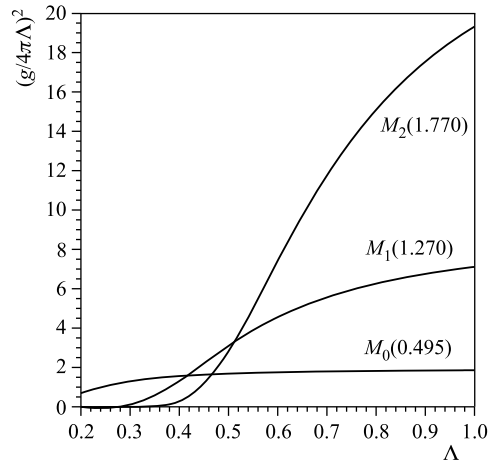


Fig. 2. The dependence $\Lambda = \Lambda(\alpha)$ evaluated from the mass equation for three different two-particle bound states with $l = 0$, $M_0 = 0.495$ GeV; $l = 1$, $M_1 = 1.270$ GeV and $l = 2$, $M_2 = 1.770$ GeV. Here we use quark masses $m_u = 0.010$ GeV and $m_s = 0.100$ GeV
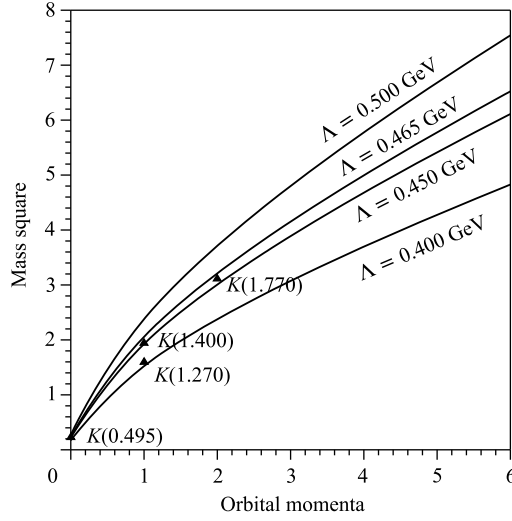
Fig. 3. The Regge trajectories of the two-particle bound states calculated for $\alpha = 1.7$ at different values of $\Lambda$ to compare with experimental evidence (triangles) of the $K$-meson family. Hereby, we plot both $K(1.270)$ and $K(1.400)$ at $l = 1$ because the RPP assignment table lists $K_{1B}$ as a mixture of these states

experimentally observed mesonic Regge trajectories. Note, these curves deform slightly when the initial «quark» masses vary in wide ranges: $m_u \in (0.010, 0.100)$ and $m_s \in (0.100, 0.450)$.

Further, the RTs or the dependence of $M_l^2 = M_l^2(l)$ on $l$ for the $K$-meson family for $\alpha = 1.7$, $m_u = 0.010$, and $m_s = 0.100$ at different values of $\Lambda \in (0.400, 0.500)$ are plotted in Fig. 3. One can see that the RTs are far not linear for lower values of $l = 0$–4, although the linearity occurs asymptotically for sufficiently large $l$. Besides, the curvature of these RTs and their slopes depend on $\Lambda$ considerably. The asymptotical behavior of the RTs for large $l$ can be obtained analytically and coincides with the exact solution of the Virton Model (20) as follows:

$$M_l^2 \sim l \cdot 2\Lambda^2 \ln(2 + \sqrt{3}) \quad \text{for} \quad l \to \infty. \tag{32}$$

A recent analysis of experimental data shows (see [23]) that the RTs of different meson and baryon families are approximately linear and their slopes slightly deviate around a constant value, although the quark configurations and quantum numbers of these hadronic families are considerably different. Note, the analyzed experimental data in [23] are available for low orbital momenta $l = 0$–3 only. Nevertheless, one can conclude that the slope of RTs weakly depends on specific details of hadron internal dynamics and may be considered as a universal characteristic which is dictated by the general properties of quark–

gluon interactions. Precisely this qualitative picture takes place in our models with AC. Thus, we have sufficient grounds to claim that the AC realizes these general properties and leads to the approximate linearity of RTs for meson families.

In conclusion, the analytic confinement in the weak coupling regime explains qualitatively the main features of meson spectra. Note, these simple models do not contain the real quantum degrees of freedom of quarks and gluons (color, flavor, spin) as well as the mechanism of the chiral symmetry breaking and, therefore, cannot pretend to describe quantitatively all details of the meson spectroscopy. The last remark: the obtained value of the coupling constant $\alpha$ in (31) is not relatively weak; however, our qualitative analysis shows that the introduction of $N$ additional quark degrees of freedom leads to the substitution $\alpha \to N\alpha_s$ so that the «effective» value of the input coupling constant $\alpha_s$ decreases almost in $N$ times. More careful consideration in this direction is the object of our next investigations.

### 3. MESONS AND GLUEBALLS

Above, it is shown that a «toy» model of interacting scalar «quarks» and «gluons» with AC could result in qualitatively reasonable description of the two- and three-particle bound states [44], and obtained analytic solutions to the ladder BSE lead to the known Regge behaviors of meson spectra [45].

Now we consider a more realistic model introduced in [46] by taking into account the spin, color, and flavor degrees of constituents. This model was further modified in [47], applied to leptonic decay constants in [48], and used to simultaneously compute meson masses and estimate the mass of the lowest-lying glueball in [34,49]. Here the aim is to collect all necessary formulae, explain the method in detail, and show that the correct symmetry structure of the quark–gluon interaction in the confinement region reflected in simple forms of the quark and gluon propagators can result in quantitatively reasonable estimates of physical characteristics in low-energy particle physics. In doing so, we build a model describing hadrons as relativistic bound states of quarks and gluons and calculate with reasonable accuracy the hadron important characteristics such as the lowest glueball mass, mass spectra of conventional mesons, and the decay constants of light mesons.

**3.1. Two-Particle Bound States.** Because of the complexity of QCD, it is often prudent to examine simpler systems exhibiting similar characteristics first. Consider a simple relativistic quantum-field model of quark–gluon interaction assuming that the AC takes place. The model Lagrangian reads [49]:

$$\mathcal{L} = -\frac{1}{4}\left(F_{\mu\nu}^A - gf^{ABC}\mathcal{A}_\mu^B \mathcal{A}_\nu^C\right)^2 + \sum_f \left(\bar{q}_f^a \left[\gamma_\alpha \partial^\alpha - m_f + g\Gamma_C^\alpha \mathcal{A}_\alpha^C\right]^{ab} q_f^b\right),$$

(33)

where $\mathcal{A}_\alpha^C$ — gluon adjoint representation ($\alpha = \{1,\ldots,4\}$); $F_{\mu\nu}^A = \partial^\mu \mathcal{A}_\nu^A - \partial^\nu \mathcal{A}_\mu^A$; $f^{ABC}$ — the $SU_c(3)$ group structure constant ($\{A,B,C\} = \{1,\ldots,8\}$); $q_f^a$ — quark spinor of flavor $f$ with color $a = \{1,2,3\}$ and mass $m_f$; $g$ — the coupling strength, $\Gamma_C^\alpha = i\gamma_\alpha t^C$; and $t^C$ — the Gell-Mann matrices.

Consider the partition function

$$Z(g) = \int \int \mathcal{D}\bar{q}\mathcal{D}q \int \mathcal{D}\mathcal{A} \exp\left\{-\int dx\, \mathcal{L}[\bar{q},q,\mathcal{A}]\right\}, \quad Z(0) = 1. \qquad (34)$$

We allow that the coupling remains of order 1 (i.e., $\alpha_s = g^2/4\pi \sim 1$) in the hadronization region. Then, the consideration may be restricted within the ladder approximation sufficient to estimate the spectra of two-quark and two-gluon bound states with reasonable accuracy [47,49]. The path integrals defining the leading-order contributions to the two-quark and two-gluon bound states read:

$$Z_{q\bar{q}} = \int \int \mathcal{D}\bar{q}\mathcal{D}q \exp\left\{-(\bar{q}S^{-1}q) + \frac{g^2}{2}\langle(\bar{q}\Gamma\mathcal{A}q)(\bar{q}\Gamma\mathcal{A}q)\rangle_D\right\}, \qquad (35)$$

$$Z_{\mathcal{A}\mathcal{A}} = \left\langle \exp\left\{-\frac{g}{2}(f\mathcal{A}\mathcal{A}F)\right\}\right\rangle_D,$$

$$\langle(\bullet)\rangle_D \doteq \int \mathcal{D}\mathcal{A} \exp\left[-\frac{1}{2}(\mathcal{A}D^{-1}\mathcal{A})\right](\bullet). \qquad (36)$$

Our model has a minimal number of parameters, namely, the coupling constant $\alpha_s$, the scale of confinement $\Lambda$, and the quark masses $\{m_{ud}, m_s, m_c, m_b\}$. Hereby, we do not make a distinction of the masses of the lightest quarks, so $m_u = m_d = m_{ud}$.

*3.1.1. Quark–Antiquark Pairs.*  Below we shortly introduce the basic steps entering into our model on the example of the quark–antiquark bound states [35] defined by $Z_{q\bar{q}}$ in (36).

First, we allocate the one-gluon exchange between colored biquark currents

$$L_2 = \frac{g^2}{2}\sum_{f_1 f_2} \int \int dx_1\, dx_2 \left(\bar{q}_{f_1}(x_1)i\gamma_\mu t^A q_{f_1}(x_1)\right) \times$$

$$\times D_{\mu\nu}^{AB}(x_1,x_2)\left(\bar{q}_{f_2}(x_2)i\gamma_\nu t^B q_{f_2}(x_2)\right). \qquad (37)$$

The color-singlet combination is isolated:

$$(t^A)^{ij}\delta^{AB}(t^B)^{j'i'} = \frac{4}{9}\delta^{ii'}\delta^{jj'} - \frac{1}{3}(t^A)^{ii'}(t^A)^{jj'}.$$

We perform a Fierz transformation

$$(i\gamma_\mu)\delta^{\mu\nu}(i\gamma_\nu) = \sum_J C_J O_J\, O_J, \quad J = \{S,P,V,A,T\},$$

where $C_J = \{1, 1, 1/2, -1/2, 0\}$ and $O_J = \{I, i\gamma_5, i\gamma_\mu, \gamma_5\gamma_\mu, i[\gamma_\mu, \gamma_\nu]/2\}$.

For systems consisting of quarks with different masses it is important to pass to the relative co-ordinates $(x, y)$ in the center-of-masses system:

$$x_1 = x + \xi_1 y, \quad x_2 = x - \xi_2 y, \quad \xi_i = \frac{m_{f_i}}{m_{f_1} + m_{f_2}}, \quad i = 1, 2.$$

Then, we rewrite (37)

$$L_2 = \frac{2g^2}{9} \sum_{J f_1 f_2} C_J \int \int dx\, dy \mathcal{J}_{J f_1 f_2}(x, y) D(y) \mathcal{J}^\dagger_{J f_1 f_2}(x, y), \qquad (38)$$

where

$$\mathcal{J}_{J f_1 f_2}(x, y) = \left(\bar{q}_{f_1}(x + \xi_1 y)\, O_J\, q_{f_2}(x - \xi_2 y)\right).$$

Introduce a system of orthonormalized basis functions $\{U_Q(x)\}$, where $Q = \{n_r, l, \mu\}$ — the radial, orbital, and magnetic quantum numbers as follows:

$$\int dx\, U_Q(x)\, U_{Q'}(x) = \delta^{QQ'}, \quad \sum_Q U_Q(z)\, U_Q(y) = \delta(z - y).$$

Expand the biquark nonlocal current on the basis

$$D(y)\mathcal{J}^\dagger_{J f_1 f_2}(x, y) = \sqrt{D(y)} \int dz\, \delta(z - y) \sqrt{D(z)} \mathcal{J}^\dagger_{J f_1 f_2}(x, z) =$$

$$= \sum_Q \int dz\, \sqrt{D(y)} U_Q(y) \sqrt{D(z)} U_Q(z)\, \mathcal{J}^\dagger_{J f_1 f_2}(x, z).$$

We define a vertex function $V_{QJ}(x, y)$

$$\bar{q}_{f_1}(x) V_{QJ}(x, y) q_{f_2}(x) \doteq \frac{2}{3} \sqrt{C_J} \sqrt{D(y)}\, U_Q(y) \bar{q}_{f_1}(x + \xi_1 y) O_J q_{f_2}(x - \xi_2 y)$$

and a colorless biquark current localized at the center of masses:

$$\mathcal{J}_{\mathcal{N}}(x) \doteq \int dy\, \left(\bar{q}_{f_1}(x)\, V_{QJ}(x, y)\, q_{f_2}(x)\right), \quad \mathcal{J}^\dagger_{\mathcal{N}}(x) = \mathcal{J}_{\mathcal{N}}(x),$$

$$\mathcal{N} = \{Q, J, f_1, f_2\}.$$

Diagonalize $L_2$ on basis $\{U_Q(x)\}$, and then (38) can be rewritten as follows:

$$L_2 = \frac{g^2}{2} \sum_{\mathcal{N}} \int dx\, \mathcal{J}_{\mathcal{N}}(x)\, \mathcal{J}_{\mathcal{N}}(x).$$

We use a Gaussian path-integral representation for the exponential

$$\exp\left(\frac{g^2}{2}\sum_{\mathcal{N}}(\mathcal{J}_{\mathcal{N}}^2)\right) = \langle \mathrm{e}^{g(B_{\mathcal{N}}\mathcal{J}_{\mathcal{N}})}\rangle_B,$$

$$\langle(\bullet)\rangle_B \doteq \int \prod_N \mathcal{D}B_N \, \exp\left[-\frac{1}{2}(B_{\mathcal{N}}^2)\right](\bullet), \quad \langle 1\rangle_B = 1$$

by introducing auxiliary meson fields $B_{\mathcal{N}}(x)$. Then,

$$Z_{q\bar{q}} = \left\langle \int\int \mathcal{D}\bar{q}\,\mathcal{D}q\, \exp\left\{-(\bar{q}S^{-1}q) + g(B_{\mathcal{N}}\mathcal{J}_{\mathcal{N}})\right\}\right\rangle_B.$$

Now we can take explicit path integration over quark variables and obtain

$$Z_{q\bar{q}} \to Z = \langle \exp\{\mathrm{Tr}\ln[1 + g(B_{\mathcal{N}}V_{\mathcal{N}})S]\}\rangle_B,$$

where $\mathrm{Tr} \doteq \mathrm{Tr}_c\,\mathrm{Tr}_\gamma \sum_{\pm}$; $\mathrm{Tr}_c$ and $\mathrm{Tr}_\gamma$ are traces taken on color and spinor indices, correspondingly, while $\sum_{\pm}$ implies the sum over self-dual and antiself-dual modes.

**3.2. Meson Ground-State Spectrum.** In particle accelerators, scientists see «jets» of many color-neutral particles in detectors instead of seeing the individual quarks. This process is commonly called hadronization and is one of the least understood processes in particle physics.

We introduce a *hadronization Ansatz* and will identify $B_{\mathcal{N}}(x)$ fields with mesons carrying quantum numbers $\mathcal{N}$. We isolate all quadratic field configurations ($\sim B_{\mathcal{N}}^2$) in the «kinetic» term and rewrite the partition function for mesons [47]:

$$Z = \int \prod_{\mathcal{N}} \mathcal{D}B_{\mathcal{N}} \, \exp\left\{-\frac{1}{2}\sum_{\mathcal{N}\mathcal{N}'}(B_{\mathcal{N}}[\delta^{\mathcal{N}\mathcal{N}'} + \Pi_{\mathcal{N}\mathcal{N}'}]B_{\mathcal{N}'}) - W_{\mathrm{res}}[B_{\mathcal{N}}]\right\}, \quad (39)$$

where the interaction between mesons is described by the residual part $W_{\mathrm{res}}[B_{\mathcal{N}}] \sim 0(B_{\mathcal{N}}^3)$.

The leading-order term of the polarization operator is

$$\alpha_s\lambda_{\mathcal{N}\mathcal{N}'}(z) \doteq \int\int dx\,dy\, U_{\mathcal{N}}(x)\alpha_s\lambda_{JJ'}(z,x,y)U_{\mathcal{N}'}(y), \quad (40)$$

and the Fourier transform of its kernel reads

$$\alpha_s\lambda_{JJ'}(p,x,y) \doteq \alpha_s\int dz\,\mathrm{e}^{ipz}\lambda_{JJ'}(z,x,y) =$$

$$= \frac{4g^2\sqrt{C_J\,C_{J'}}}{9}\sqrt{D(x)D(y)}\int \frac{d^4k}{(2\pi)^4}\,\mathrm{e}^{-ik(x-y)}\times$$

$$\times \mathrm{Tr}\left[O_J\tilde{S}_{m_1}(\hat{k}+\xi_1\hat{p})O_{J'}\tilde{S}_{m_2}(\hat{k}-\xi_2\hat{p})\right]. \quad (41)$$

The Bethe–Salpeter (BS) equation is an important tool for studying the relativistic two-particle bound states in a field theory framework [21]. Numerical calculations indicate that the ladder BS equation with a phenomenological model can give satisfactory results (for a review, see [22]). Particularly, a BS formalism adjusted for QCD was developed to extract values of $\alpha_s$ below 1 GeV by comparison with known meson masses [50].

We diagonalize the polarization kernel on the orthonormal basis $\{U_\mathcal{N}\}$:

$$\int \int dx\, dy\, U_\mathcal{N}(x) \lambda_{JJ'}(p,x,y)\, U_{\mathcal{N}'}(y) = \delta^{\mathcal{N}\mathcal{N}'} \lambda_\mathcal{N}(-p^2)$$

that is equivalent to the solution of the corresponding ladder BSE. We rewrite:

$$\lambda_\mathcal{N}(-p^2) = \frac{8C_J}{3\pi^3} \int d^4k\, |V_J(k)|^2\, \Pi_\mathcal{N}(k,p),$$

$$V_J(k) \doteq \int d^4x\, U_J(x)\sqrt{D(x)}\, \mathrm{e}^{-ikx}, \tag{42}$$

$$\Pi_\mathcal{N}(k,p) \doteq \frac{1}{24}\mathrm{Tr}\left[O_J \tilde{S}_{m_1}\left(\hat{k} + \xi_1\hat{p}\right) O_{J'} \tilde{S}_{m_2}\left(\hat{k} - \xi_2\hat{p}\right)\right],$$

where, $V_J(k)$ is a vertex and $\Pi_\mathcal{N}(k,p)$ is the kernel of the polarization operator.

In relativistic quantum-field theory, a stable bound state of $n$ massive particles shows up as a pole in the $S$ matrix with a center-of-mass energy. Accordingly, the physical mass of meson may be derived from the equation:

$$1 + \alpha_s \lambda_\mathcal{N}(M_\mathcal{N}^2) = 0, \quad -p^2 = M_\mathcal{N}^2. \tag{43}$$

Then, with a renormalization

$$(B_\mathcal{N}[1 + \alpha_s \lambda_\mathcal{N}(-p^2)]B_\mathcal{N}) =$$
$$= (B_\mathcal{N}[1 + \alpha_s \lambda_\mathcal{N}(M_\mathcal{N}^2) + \alpha_s \dot{\lambda}_\mathcal{N}(M_\mathcal{N}^2)[p^2 + M_\mathcal{N}^2]B_\mathcal{N}) =$$
$$= (B_R[p^2 + M_\mathcal{N}^2]B_R), \quad (44)$$

$$\dot{\lambda}_\mathcal{N}(z) \doteq \frac{d\lambda_\mathcal{N}(z)}{dz}, \quad B_R(x) \doteq \sqrt{\alpha_s \dot{\lambda}_\mathcal{N}(M_\mathcal{N}^2)}B_\mathcal{N}(x)$$

the partition function takes the conventional form:

$$Z = \int \mathcal{D}B_R\, \exp\left\{-\frac{1}{2}\left(B_R\left[p^2 + M_\mathcal{N}^2\right]B_R\right) - W_\mathrm{res}[B_R]\right\}. \tag{45}$$

The use of the path-integral technique leads to the following practical advantages over simply solving a BSE with one-boson exchange:

(i) The vacuum functional may be written in alternative representations, either through original variables of quarks and gluons, or in terms of bound states, i.e., we obtain the so-called «quark–hadron duality».

(ii) The BS kernel (41) is natively obtained in a symmetric form.

(iii) The normalization of the operators of bound states is performed in the most simple way by keeping the condition $\dot{\lambda}(M_J) > 0$ evident.

(iv) After renormalization (44) the partition function of the system of $B_{\mathcal{N}}$ fields takes the conventional form with a kinetic term and interaction parts.

*3.2.1. Pseudoscalar and Vector Mesons.* In the quark model $(q_{f_1}\bar{q}_{f_2})$ bound states are classified in $J^{PC}$ multiplets. For a pair with spin $s = \{0, 1\}$ and angular momentum $\ell$, the parity is $P = (-1)^{\ell+s}$, and the total spin is $|\ell - s| < J < |\ell + s|$.

Below we consider the most established sectors of hadron spectroscopy, the meson ground states ($\ell = 0, n_r = 0$), namely, the pseudoscalar $\mathbf{P}(0^{-+})$ and vector $\mathbf{V}(1^{--})$ mesons.

We should derive the meson masses from (42). The polarization kernel $\lambda_{\mathcal{N}}(-p^2)$ is real and symmetric that allows us to find a simple variational solution to this problem. For the ground-state trial function $U_0(x)$ we choose [35]:

$$U_{01}(x, a) \sim \sqrt{D(x)} \exp\left\{-\frac{a\Lambda^2 x^2}{4}\right\}, \quad \int dx \, |U_{01}(x, a)|^2 = 1, \quad a > 0. \quad (46)$$

After substituting (46) into (42), the variational equation defining the masses of $\mathbf{P}$ and $\mathbf{V}$ mesons is as follows:

$$1 = -\alpha_s \lambda_J(\Lambda, M_J, m_1, m_2) =$$
$$= \frac{\alpha_s C_J \Lambda^2}{3\pi m_1 m_2} \exp\left\{\frac{M_J^2(\xi_1^2 + \xi_2^2) - m_1^2 - m_2^2}{2\Lambda^2}\right\} \times$$
$$\times \max_{1/4 < a < 1/2} \left\{\left[\frac{(6a-1)(1-2a)}{a}\right]^2 \times \right.$$
$$\times \exp\left[-\frac{aM_J^2(\xi_1 - \xi_2)^2}{2\Lambda^2}\right]\left[4a\rho_J + \frac{M_J^2}{\Lambda^2}\left(\xi_1\xi_2 + a(2 - a\rho_j)(\xi_1 - \xi_2)^2\right) + \right.$$
$$\left.\left. + \frac{m_1 m_2}{\Lambda^2}\left[1 + \chi_J \omega(m_1)\omega(m_2)\right]\right]\right\}, \quad (47)$$

where $C_J = \{1, 1/2\}$, $\rho_J = \{1, 1/2\}$ and $\chi_J = \{1, -1\}$ for $J = \{P, V\}$.

Localization of the meson field at the center of masses of two quarks results in the following asymptotic properties. For mesons consisting of two very heavy quarks ($m_1 = m_2 = m \gg 1$) we solve (47) and obtain the correct asymptotic behavior

$$M_J^2 = 4m^2 + \varepsilon_J, \quad \varepsilon_J \doteq 4\ln\left(\frac{3\pi}{32(7 - 4\sqrt{3})\,C_J\alpha_s}\right).$$

Note, the next-to-leading value $\varepsilon_J$ does not depend on any masses. Moreover, $\varepsilon_V > \varepsilon_P$, because the corresponding Fierz coefficients obey $C_P = 1 > C_V = 1/2$. The mass splitting $M_V > M_P$ remains for «heavy–heavy» quarkonia.

For a «heavy-light» quarkonium ($m_1 \gg 1$, $m_2 \sim 1$) we estimate the mass

$$M_J^2 = m_1^2 - \epsilon_J, \quad \epsilon_J \neq \epsilon_J(M_J).$$

To calculate the meson masses we need to fix the model parameters. We determine the quark mass $m_{ud}$ and the coupling constant $\alpha_s$ from equations:

$$1 + \alpha_s \lambda_P(\Lambda, 138 \,\text{MeV}, m_{ud}, m_{ud}) = 0, \quad 1 + \alpha_s \lambda_V(\Lambda, 770, m_{ud}, m_{ud}) = 0 \quad (48)$$

by fitting the well-established mesons $\pi(138)$ and $\rho(770)$ at different values of $\Lambda$. The remaining constituent quark masses $m_s, m_c$, and $m_b$ are determined by fitting the known mesons $K(495)$, $J/\Psi(3097)$, and $\Upsilon(9460)$ as follows:

$$1 + \alpha_s \lambda_P(\Lambda, 495, m_{ud}, m_s) = 0,$$
$$1 + \alpha_s \lambda_V(\Lambda, 3097, m_c, m_c) = 0,$$
$$1 + \alpha_s \lambda_V(\Lambda, 9460, m_b, m_b) = 0.$$

The dependencies of the constituent quark masses $m_q$ and estimated meson masses $M$ on $\Lambda$ are plotted in Figs. 4 and 5, correspondingly.

The sharp drop of all quark mass curves in Fig. 4 may be shortly explained as follows. Note, two equations in (48) mostly differ by meson masses in exponentials along different numerical factors $C_J$, $\rho_J$, and $\chi_J$. They have general
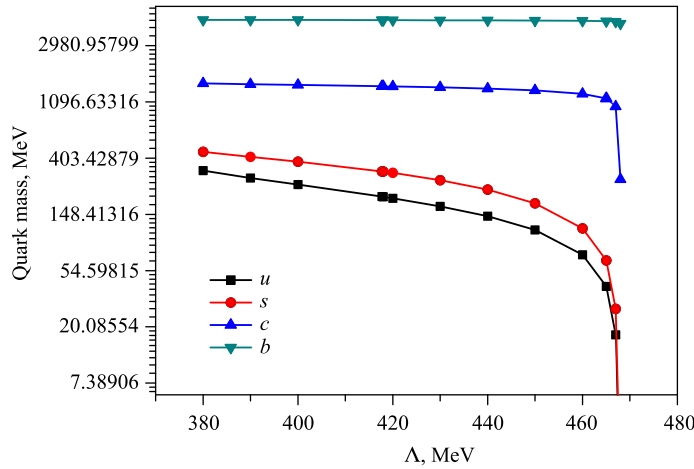


Fig. 4. Solutions for constituent quark masses vers. the confinement scale value $\Lambda$
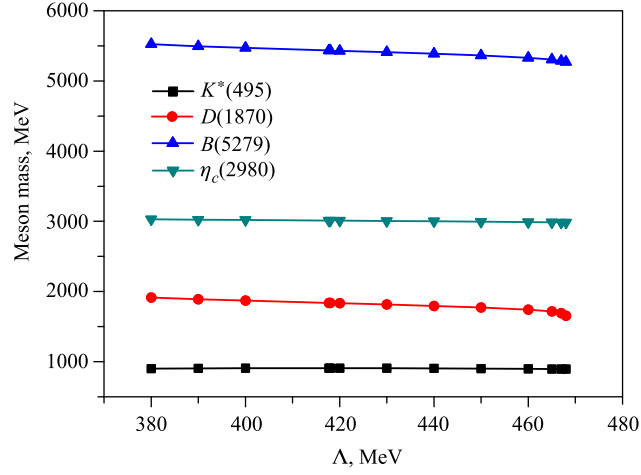
Fig. 5. Solutions for some meson masses in dependence on the confinement scale value $\Lambda$

solutions $\{m_{ud}, \alpha_s\}$ not for any $\Lambda$. Suppose, at fixed $\Lambda = \Lambda_0$ they are solvable. Then, for finite coupling $\alpha_s$, the solution $m_{ud}$ is obviously finite to obey both equations. However, for vanishing $\alpha_s \to 0$ the equations take the form

$$1 \approx \frac{\alpha_s C_J}{m_{ud}^2} \text{const}\,(\Lambda_0, M_J, \rho_J),$$

and the solution for quark mass behaves $m_{ud} \sim \sqrt{\alpha_s} \to 0$. Exactly this behavior is observed in Fig. 4.

By using these quark masses and coupling constant we can estimate other meson masses in dependence on $\Lambda$, and some results are shown in Fig. 6.

To fix the value of parameter $\Lambda$ we calculate the weak decay constants $f_\pi$ and $f_K$ to compare with experimental data. Note, these constants considerably depend on $\Lambda$ (see Fig. 7) that allow us to fix it unambiguously at $\Lambda = 416.4$ MeV.

The final set of model parameters are fixed as follows:

$$\alpha_s = 1.5023, \quad \Lambda = 416.4 \text{ MeV}, \quad m_{ud} = 206.9 \text{ MeV},$$
$$m_s = 323.6 \text{ MeV}, \quad m_c = 1453.8 \text{ MeV}, \quad m_b = 4698.9 \text{ MeV}. \tag{49}$$

With these parameters we have estimated the pseudoscalar and vector meson masses shown in Fig. 6 and compared with experimental data [12]. The relative error of our estimate does not exceed 3.5 per cent in the whole range of mass (from 0.14 up to 9.5 GeV).

There are mainly two schemes describing $\omega - \Phi$ and $\eta - \eta'$ mixing [12]. The octet-singlet scheme uses the mixing angle $\theta$ between states $(u\bar{u} + d\bar{d} - 2s\bar{s})/\sqrt{6}$ and $(u\bar{u} + d\bar{d} + s\bar{s})/\sqrt{3}$. We use the quark-flavor based mixing scheme between
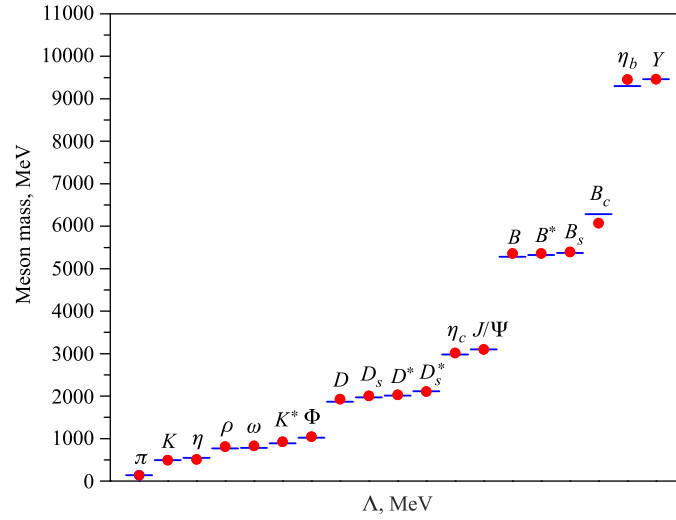
Fig. 6. Estimated masses (dots) of conventional mesons (in units of MeV) compared with experimental data (lines) from PDG-2008



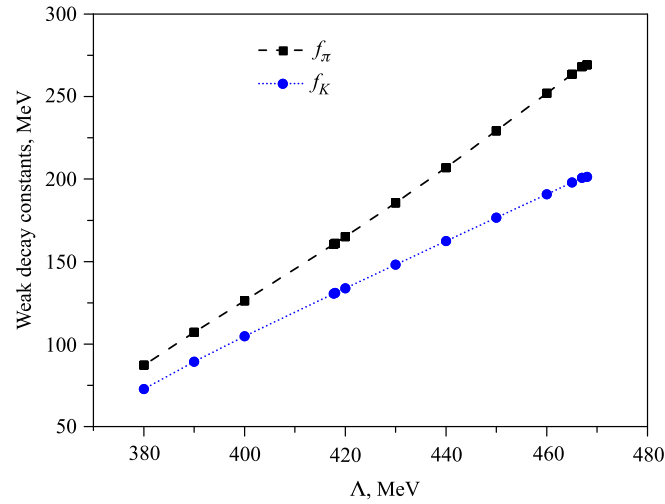Fig. 7. Weak decay constants vers. the confinement scale value $\Lambda$

states $(u\bar{u} + d\bar{d})/\sqrt{2}$ and $s\bar{s}$ with mixing angle $\varphi$. These two schemes are equivalent to each other by $\theta = \varphi - \pi/2 + \arctan{(1/\sqrt{2})}$, when the $SU(3)$ symmetry is perfect. Particularly, for «ideal» vector mixing the angle is $\varphi_V^{\mathrm{id}} = 90°$ or $\theta_V^{\mathrm{id}} = 35.3°$.

With fixed parameters (49) we calculate a relatively heavy mass $M_V(s\bar{s}) = 1064$ MeV of vector $s\bar{s}$ state. To obtain correct masses of $\omega(782)$ and $\Phi(1019)$ one needs a considerable mixing to the light quark–antiquark state with mixing angle $\varphi_V \simeq 73.2°$ which differs significantly from the «ideal» value. By using the same parameters (49) we obtain a pseudoscalar $s\bar{s}$ state with mass $M_P(s\bar{s}) = 705$ MeV. We cannot describe the physical mass of $\eta'(958)$ by any mixing to the light-quark pair and can only fit the correct mass $M_P(\eta) = 547$ MeV at angle $\varphi_P \simeq 58.5°$. Our model fails to describe simultaneously the $\eta - \eta'$ mixing. This problem obviously deserves a separate consideration.

Note, the infrared behavior of effective (mass-dependent) QCD coupling $\alpha_s$ is not well defined and needs to be more specified [39,51,52]. In the region below the $\tau$-lepton mass ($M_\tau = 1.777$ GeV), the strong-coupling value is expected between $\alpha_s(M_\tau) \approx 0.34$ [12] and the infrared fix point $\alpha_s(0) = 2.972$ [53]. Our parameter $\alpha_s = 1.5023$ does not contradict this expectation because it is estimated to fit the $\pi$-meson mass, and so the corresponding energy scale is $\sim 140$ MeV. We keep this value for further calculations.

**3.3. Weak Decay Constants.** An important quantity in the meson physics is the weak decay constant. The precise knowledge of its value provides great improvement in our understanding of various processes convolving meson decays. For the pseudoscalar mesons, the weak decay constant $f_P$ is defined by the following current-meson duality:

$$i f_P\, p_\mu = \langle 0|J_A(0)|U_R(p)\rangle,$$

where $J_A$ is the axial vector part of the weak current and $U_R(p)$ is the normalized vector of state.

We estimate

$$
\begin{aligned}
f_P \cdot p_\mu &= \frac{\sqrt{2}\,g}{3} \int \frac{dk}{(2\pi)^4} \int dx\, \mathrm{e}^{-ikx}\, U_R(x)\sqrt{D(x)} \times \\
&\quad \times \mathrm{Tr}\left[ i\gamma_5 \tilde{S}\left(\hat{k} + \xi_1\hat{p}\right) \gamma_5\gamma_\mu \tilde{S}\left(\hat{k} - \xi_2\hat{p}\right)\right] = \\
&= p_\mu \frac{32\Lambda\alpha_s\sqrt{2\dot{\lambda}(M_P^2)}}{3\pi^{3/2}(m_1 + m_2)} \frac{(1 - 2a_P)(6a_P - 1)}{(1 + 2a_P)^2} \times \\
&\quad \times \left[ 1 + \frac{a_P}{1 + 2a_P} \frac{(m_1 - m_2)^2}{m_1 m_2} \right] \times \\
&\quad \times \exp\left[ \frac{M_J^2(\xi_1^2 + \xi_2^2) - m_1^2 - m_2^2}{2} - \frac{a_P}{1 + 2a_P} M_P^2(\xi_1 - \xi_2)^2 \right], \quad (50)
\end{aligned}
$$

where $a_P$ is the value of parameter $a$ calculated for the given meson with mass $M_{\mathbf{P}}$.

Particularly, for an «asymmetric» meson containing an infinitely heavy quark ($m_1 \gg m_2 \sim 1$) we obtain the correct asymptotic behavior

$$f_P \sim 1/\sqrt{m_1}$$

due to the localization of the meson field at the center of two quark masses.

The weak decay constants of light mesons are well established data and many groups (MILC [54], NPLQCD [55], HPQCD [56], etc.) have these with accuracy at the 2 percent level. Therefore, these values are often used to test any model in QCD. By substituting optimal values of $\{m_{ud}, m_s, \alpha_s, \Lambda\}$ (49) into (50) we calculate

$$f_\pi = 128.8 \text{ MeV}, \quad f_K = 157.7 \text{ MeV}.$$

Our estimates are in agreement with the experimental data [12, 57]:

$$f_{\pi^-}^{\text{PDG}} = (130.4 \pm 0.04 \pm 0.2) \text{ MeV}, \quad f_{K^-}^{\text{PDG}} = (155.5 \pm 0.2 \pm 0.8 \pm 0.2) \text{ MeV}.$$
$$(51)$$

Our model represents a reasonable framework to describe the conventional mesons, and the parameters are fixed. Below we can consider two-gluon bound states.

**3.4. Glueballs.** Because of the confinement, gluons are not observed, they may only come in bound states called *glueballs*. Glueballs are the most unusual particles predicted by the QCD but not found experimentally yet [58]. There are predictions expecting non-$q\bar{q}$ scalar objects, like glueballs, and multiquark states in the mass range $\sim 1500{-}1800$ MeV [59, 60]. Experimentally the closest scalar resonances to this energy range are the $f_0(1500)$ and $f_0(1710)$ [61]. Some references favor the $f_0(1500)$ as the lightest scalar glueball [62], while others do so for the $f_0(1710)$ [63,64]. Recent scalar hadron $f_0(1810)$ reported by the BES Collaboration may also be a glueball candidate [65].

The study of glueballs currently deserves much interest from a theoretical point of view, either within the framework of effective models or lattice QCD. The glueball spectrum has been studied by using effective approaches like the QCD sum rules [66], Coulomb gauge QCD [67], and potential models (e.g., [68, 69]), etc. The potential models consider glueballs as bound states of two or more constituent gluons interacting via a phenomenological potential [68, 70, 71]. It should be noted that potential models have difficulties in reproducing all known lattice QCD data. Different string models are used for describing glueballs [72, 73], including combinations of string and potential approaches [69]. It has been shown that a proper inclusion of the helicity degrees of freedom can improve the compatibility between lattice QCD and potential models [74].

An important theoretical achievement in this field has been the prediction and computation of the glueball spectrum in lattice QCD simulations [75, 76]. Recent

lattice calculations, QCD sum rules, «tube» and constituent glue models predict that the lightest glueball has the quantum numbers of scalar ($J^{PC} = 0^{++}$) and tensor ($2^{++}$) states [77]. Gluodynamics has been extensively investigated within quenched lattice QCD simulations and the lightest glueball is found a scalar object with a mass of $\simeq (1.66 \pm 0.05)$ GeV [78]. A use of much finer isotropic lattices resulted in a value 1.475 GeV [76]. Recently, an improved quenched lattice calculation of the glueball spectrum at the infinite volume and continuum limits based on much larger and finer lattices have been carried out and the scalar glueball mass is calculated to be $(1710 \pm 50 \pm 80)$ MeV [79].

Two-gluon bound states are the most studied purely gluonic systems in the literature, because when the spin-orbital interaction is ignored ($\ell = 0$), only scalar and tensor states are allowed. Particularly, the lightest glueballs with positive charge parity can be successfully modeled by a two-gluon system in which the constituent gluons are massless helicity-one particles [80].

Below we consider a two-gluon scalar bound state. We isolate the color-singlet term in the bigluon current in $Z_{\mathcal{AA}}$ (36) by using the known relations

$$t^C_{ik}\, t^C_{jl} = \frac{N_c^2 - 1}{2N_c^2}\delta^{il}\delta^{jk} - \frac{1}{N_c}t^C_{il}t^C_{jk},$$

$$f^{ABE}f^{A'B'E} = \frac{2}{3}\left(\delta^{AA'}\delta^{BB'} - \delta^{AB'}\delta^{BA'}\right) + d^{AA'E}d^{BB'E} - d^{AB'E}d^{BA'E}.$$

The second-order matrix element containing a color-singlet two-gluon current reads [49]

$$L_{\mathcal{AA}} = \frac{g^2}{4 \cdot 3} \int \int dx\, dy\, \left( J^{AA}_{\mu\mu'}(x,y)J^{BB}_{\nu\nu'}(x,y) - J^{AA}_{\mu\nu'}(x,y)J^{BB}_{\nu\mu'}(x,y) \right) \times$$

$$\times \left[ \delta^{\nu\nu'} W_{\mu\mu'}(x,y) - \delta^{\mu\nu'} W_{\nu\mu'}(x,y) - \delta^{\nu\mu'} W_{\mu\nu'}(x,y) + \delta^{\mu\mu'} W_{\nu\nu'}(x,y) \right],$$

where

$$J^{BC}_{\mu\nu}(x,y) \doteq \mathcal{A}^B_\mu(x)\mathcal{A}^C_\nu(y),$$

$$W_{\mu\nu}(x,y) \doteq \frac{\partial}{\partial x_\mu}\frac{\partial}{\partial y_\nu}D(x - y) = \delta^{\mu\nu}\, W(x - y) + \dots,$$

$$W(z) = \frac{1}{(2\pi)^2}\, \mathrm{e}^{-z^2}.$$

This part consists of spin-zero (scalar) and spin-two (tensor) components. Below we consider the scalar component:

$$L^S_{\mathcal{AA}} = \frac{g^2}{3} \int \int dx_1\, dx_2\, J(x_1, x_2)W(x_1 - x_2)J(x_1, x_2),$$

$$J(x_1, x_2) \doteq J^{BB}_{\mu\mu}(x_1, x_2).$$

By introducing the relative coordinates ($x_1 \doteq x + y/2$, $x_2 \doteq x - y/2$) we rewrite

$$L_{\mathcal{A}\mathcal{A}}^S = \frac{g^2}{3} \int \int dx \, dy \, J(x,y) W(y) J(x,y). \tag{52}$$

One can see that the matrix element (52) is similar to (38) by the very construction. By omitting details of intermediate calculations (similar to those represented in the previous section) we rewrite the partition function in terms of auxiliary field $B(x)$ as follows:

$$Z_{\mathcal{A}\mathcal{A}} \rightarrow Z_G = \int \mathcal{D}B \exp \left\{ -\frac{1}{2} \left( B \, G^{-1} B \right) + L_I[B] \right\},$$

where $L_I[B] \sim O(B^3)$ and the BS kernel is

$$G^{-1}(x - y) = \delta(x - y) - \frac{8g^2}{3} \Pi(x - y),$$

$$\Pi(z) \doteq \int \int dt \, ds \, U_n(t) \sqrt{W(t)} \, D\left( \frac{t+s}{2} + z \right) D\left( \frac{t+s}{2} - z \right) \sqrt{W(s)} \, U_n(s).$$

*3.4.1. Lowest-State Glueball.* The hadronization Ansatz allows us to identify $B$ with scalar glueball field. To find the glueball mass we should diagonalize the Bethe–Salpeter kernel $\Pi(z)$. The glueball mass $M_G$ is defined from equation [34]:

$$1 - \frac{8g^2}{3} \int dz \, e^{izp} \, \Pi(z) = 0, \quad p^2 = -M_G^2. \tag{53}$$

For the lightest ground-state scalar glueball choose a Gaussian wave function:

$$U(x) = \frac{2c}{\pi} \, e^{-cx^2}, \quad \int dx \, |U(x)|^2 = 1, \quad c > 0.$$

Then, we derive (53) as follows:

$$1 = \frac{\alpha_s}{\alpha_{\text{crit}}} \exp \left\{ \frac{M_G^2}{4\Lambda^2} \right\}, \quad \alpha_{\text{crit}} \doteq \frac{3\pi(3 + 2\sqrt{2})^2}{4}.$$

The final analytic result for the lowest-state glueball mass reads

$$M_G = 2\Lambda \left[ \ln \left( \frac{\alpha_{\text{crit}}}{\alpha_s} \right) \right]^{1/2}. \tag{54}$$

The solution $M_G^2 \geqslant 0$ exists for any $\alpha_s < \alpha_{\text{crit}} \approx 80.041$.

Note, the scalar glueball mass depends linearly on the confinement scale $\Lambda$, and the scaled mass $M_G/\Lambda$ depends only on coupling $\alpha_s$ (see Fig. 8). Particularly,
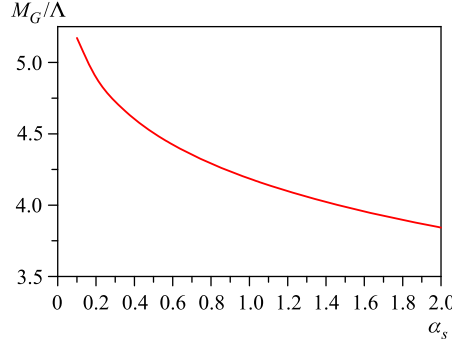
Fig. 8. Evolution of the lowest-state glueball mass scaled to $\Lambda$ with the coupling $\alpha_s$

if we take values $\Lambda \sim \Lambda_{\mathrm{QCD}} \approx 360$ MeV and $\alpha_s \simeq \alpha_s(M_\tau) = 0.343$, then we estimate $M_G \approx 1710$ MeV.

However, our purpose is to describe simultaneously different sectors of low-energy particle physics. Accordingly, with values $\alpha_s = 1.5023$ and $\Lambda = 416.4$ MeV determined by fitting the meson masses and weak decay constants, we calculate the scalar glueball mass as follows:

$$M_G = 1661 \text{ MeV}. \tag{55}$$

Our estimate (55) is in reasonable agreement with other predictions expecting the lightest glueball located in the scalar channel in the mass range $\sim 1500$–$1800$ MeV [59,66,76,81]. The often referred quenched QCD calculations predict $(1750 \pm 50 \pm 80)$ MeV for the mass of the lightest glueball [75]. The recent quenched lattice estimate with improved lattice spacing favors a scalar glueball mass $M_G = (1710 \pm 50 \pm 58)$ MeV [79].

Another important property of the scalar glueball is its size, the «radius» which should depend somehow on the glueball mass. We estimate the glueball size by using the «effective potential» $W(y)$ (52) connecting two scalar gluon currents. The glueball radius may be roughly estimated as follows

$$r_G \sim \sqrt{\frac{\int d^4 x \, x^2 \, W(x)}{\int d^4 x \, W(x)}} = \frac{\sqrt{2}}{\Lambda} \approx \frac{1}{295 \text{ MeV}} \approx 0.67 \text{ fm}. \tag{56}$$

This means that the dominant forces responsible for binding gluons must be provided by medium-sized vacuum fluctuations of correlation length $\sim 0.7$ fm. Consequently, typical energy-momentum transfers inside a scalar glueball occur at the QCD scale $\sim 360$ MeV, rather than at the chiral symmetry breaking scale $\Lambda_\chi \sim 1$ GeV (or $\sim 5$ fm).

From (54) and (56) we deduce that

$$r_G \cdot M_G = 2\sqrt{2} \left[ \ln \left( \frac{\alpha_{\text{crit}}}{\alpha_s} \right) \right]^{1/2} \approx 5.64.$$

This value may be compared with the prediction ($r_G \cdot M_G = 4.16 \pm 0.15$) of quenched QCD calculations [75, 79]. A study of the glueball properties at finite temperature using $SU(3)$ lattice QCD at the quenched level with the anisotropic lattice, imposes restrictions on the glueball parameters at zero temperature: $0.37 < r_G < 0.57$ fm and $M_G \simeq 1.49$ GeV [82]. The nonprincipal differences of quenched lattice QCD data from our estimates may be explained by the presence of quarks (our parameters have been fixed by fitting two-quark bound states) in our model.

A method of analysis of correlation functions in QCD is to calculate the corresponding condensates. The value of the correlation function dictates the values of the condensates. We calculate the lowest nonvanishing gluon condensate in the leading-order (ladder) approximation:

$$g^2 \, \mathrm{T} \, \left\langle F_{\mu\nu}^A F_A^{\mu\nu} \right\rangle = 8 N_c \pi \alpha_s \Lambda^4 \int d^4 z \, W(z) = 6\pi \alpha_s \Lambda^4 \approx 0.8 \text{ GeV}^4$$

which is the same order of magnitude with the reference value [83]

$$g^2 \, \mathrm{Tr} \, \left\langle G_{\mu\nu} G^{\mu\nu} \right\rangle \approx 0.5 \text{ GeV}^4.$$

In conclusion, the suggested model in its simple form is far from real QCD. However, our aim is to demonstrate that global properties of the lowest glueball state and conventional mesons may be explained in a simple way in the framework of a simple relativistic quantum-field model of quark–gluon interaction based on AC. Our guess about the symmetry structure of the quark–gluon interaction in the confinement region has been tested and the use of simple forms of propagators has resulted in quantitatively reasonable estimates in different sectors of the low-energy particle physics. The consideration can be extended to other problems in hadron physics.


## 4. QCD RUNNING COUPLING IN LOW-ENERGY REGION

One of the fundamental parameters of nature, the QCD effective coupling $\alpha_s$, can provide a continuous interpolation between the asymptotical free state, where perturbation theory works well, and the hadronization regime, where nonperturbative techniques must be employed.

QCD predicts the functional form of the energy dependence of $\alpha_s$ on energy scale $Q$, but its actual value at a given $Q$ must be obtained from experiment. This dependence is described theoretically by the renormalization group equations and measured at relatively high energies [84, 85]. A self-consistent and physically meaningful prediction of the QCD effective charge in the IR regime remains one of the actual problems in particle physics.

The present paper is aimed to determine the QCD effective charge in the low-energy region by exploiting the hadron spectrum. In doing so we extend our previous investigations [35, 44, 45], where we provided new, independent, analytic and numerical estimates on the lowest glueball mass, conventional meson spectrum and the weak decay constants by using a fixed («frozen») value of $\alpha_s$. The obtained results were in reasonable agreement with experimental evidence.

Below we take into account the dependence of $\alpha_s$ on mass scale $M$ and develop a phenomenological model to describe the IR behavior of $\alpha_s$. We determine the meson masses by solving the ladder Bethe–Salpeter (BS) equations for two-quark bound states. The consideration is based on a relativistic quantum-field model with AC and has a minimal number of parameters, namely, the confinement scale $\Lambda$ and the constituent quark masses $m_f$ ($f = \{ud, s, c, b\}$). First, we derive meson mass formula and adjust the model parameters by fitting heavy meson masses ($M \geqslant 2$ GeV). Hereby, we determine corresponding values of $\alpha_s(M)$ from a smooth interpolation of the newest experimental data on the QCD coupling constant. Having adjusted model parameters, we estimate $\alpha_s(M)$ in the low-energy domain by exploiting meson masses below $\sim 1$ GeV. As an application, we estimate some intermediate and heavy meson masses ($1 < M < 9.5$ GeV). Finally, we extract a specific IR-finite behavior of the QCD coupling and conclude briefly recalling the comparison with often quoted results and recent experimental data.

**4.1. Effective Coupling of QCD.** The polarization of QCD vacuum causes two opposite effects: the color charge $g$ is screened by the virtual quark–antiquark pairs and antiscreened by the polarization of virtual gluons. The competition of these effects results in a variation of the physical coupling under changes of distance $\sim 1/Q$, so QCD predicts a dependence $\alpha_s \doteq g^2/(4\pi) = \alpha_s(Q)$. This dependence is described theoretically by the renormalization group equations and determined experimentally at relatively high energies [84, 85].

Nowadays, determinations of $\alpha_s$ remain at the forefront of experimental studies and tests of QCD. Recent developments on this way were summarized in a number of articles [12, 86, 87]. Summary of the recent experimental measurements of $\alpha_s$ (Fig. 9) and particular values of $\alpha_s$ at intermediate energies (see Table 1) are given by referring to [85, 86].

Note, there are two separate $q^2$ scale regions in which a running coupling may be considered. The *spacelike* region ($q^2 = -Q^2 < 0$ with relativistic momentum transfer $Q^2$) is related to scattering processes while *timelike* domain
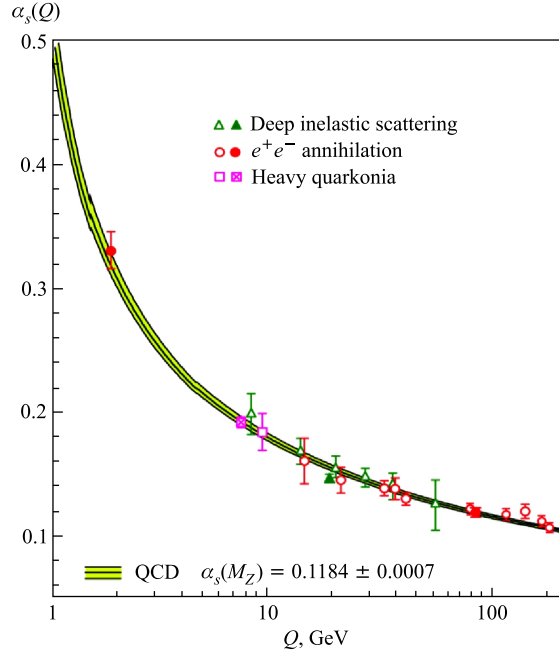
Fig. 9. Measurements of $\alpha_s$ as a function of the respective energy scale $Q$ vers. QCD predictions (curves) [86]

*Table* 1. **Some measurements of $\alpha_s$ at intermediate energies**

| Process | $Q$, GeV | $\alpha_s(Q)$ | Ref. |
|---|---|---|---|
| $\tau$-decays | 1.78 | 0.330±0.014 | [86] |
| $Q\bar{Q}$ states | 4.1 | 0.239±0.012 | [92] |
| $\Upsilon$ decays | 4.75 | 0.217±0.021 | [93] |
| $Q\bar{Q}$ states | 7.5 | 0.1923±0.0024 | [86] |
| $\Upsilon$ decays | 9.46 | 0.184±0.015 | [86] |
| $e^+e^-$ jets | 14.0 | 0.170±0.021 | [94] |

($q^2 = M^2 > 0$, where $M$ is the hadron mass) is often used for annihilation and decay processes. The consistent description of QCD effective coupling $\alpha_s$ in these domains remains the goal of many studies because only asymptotically the two definitions can be identified, but at low momentum they can be very different (see, e.g., [88]). Particularly, the behavior of one-loop analytic running coupling [89] in timelike and spacelike domains is plotted in Fig. 10.
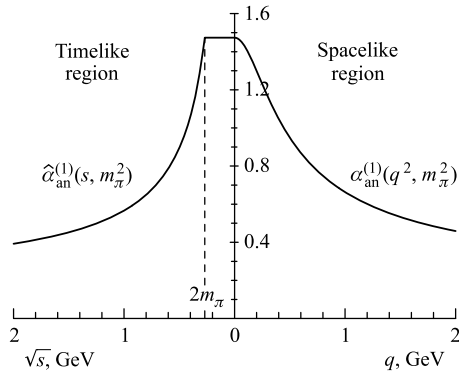
Fig. 10. The one-loop massless analytic running coupling in the spacelike and timelike domains (taken from [89])

Many quantities in hadron physics are affected by the IR behavior of the coupling in different amounts. Nevertheless, the long-distance behavior of $\alpha_s$ is not well defined, it needs to be more specified [39,51,52], and correct description of QCD effective coupling in the IR regime remains one of the actual problems in particle physics. Particularly, one of the most precise determinations of $\alpha_s$ near low-energy region is done by studying $\tau$-lepton decays reporting central values ranging from 0.318 to 0.344 [90,91].

An attempt to extrapolate the perturbative approach to the long-distance QCD has been made, it has been suggested that $\alpha_s$ freezes at a finite and moderate value [95], and this behavior could be the reason for the soft transition between short and long distance behaviors.

Different nonperturbative approaches have been proposed to deal with the IR properties of $\alpha_s$. Particularly, methods, based on gauge-invariant SDE, concluded that an IR-finite coupling constant may be obtained from first principles [96]. New solutions for the gluon and ghost SDE have been obtained with better approximations which led to a new value for the IR coupling constant at the origin [97, 98]. Many works within the lattice simulations have been devoted in the last years to the study of the QCD running coupling constant either in perturbative regime [99, 100] or in the deep IR domain [101]. Note, the results of various nonperturbative methods for the QCD invariant coupling may differ among themselves in the IR region due to the specifications of the used methods and approximations. Particularly, the results obtained by lattice simulations and SDE methods demonstrate a considerable variety of IR behaviors of $\alpha_s$.

An extraction of experimental data of $\alpha_s^{\mathrm{exp}}(Q^2)$ below 1 GeV compared with the meson spectrum within analytic perturbation theory has been performed

in [50]. The earliest attempts to obtain $\alpha_s$ in the IR region were made in the framework of the quark–antiquark potential models by using Wilson loop method [27, 102–105]. Convenient interpolation formulas between the large momentum perturbative expression and a finite IR-fix point have been used in hadron spectrum studies with $\alpha_s^0/\pi \simeq 0.19$–$0.25$ [27]. Within a fully relativistic treatment it was shown that a $\rho$-meson mass much heavier than the $\pi$ mass could be obtained with $\alpha_s^0/\pi \simeq 0.265$ [106] while a similar result within a one-loop analytic coupling method predicted $\alpha_s^0/\pi \simeq 0.44$ [107]. A phenomenological hypothesis was adopted that the gluon acquires an effective dynamical mass $m_g \approx 370$ MeV (at $\Lambda_{\mathrm{QCD}} \approx 300$ MeV) that resulted in $\alpha_s^0/\pi \simeq 0.26$ [108]. Various event shape in $e^+e^-$ annihilation can be reproduced with an averaged value $\langle \alpha_s^0/\pi \rangle \simeq 0.2$ on interval $\leqslant 1$ GeV [17].

**4.2. Conventional Meson Spectrum and Running Coupling.** We use the meson mass $M$ as the appropriate characteristic parameter, so the coupling $\hat{\alpha}_s(M)$ is defined in a timelike domain. On the other hand, the most of known data on $\alpha_s(Q)$ are possible in spacelike region. The continuation of the invariant charge from the spacelike to the timelike region (and vice versa) was elaborated by making use of the integral relationships between the QCD running coupling in Euclidean and Minkowskian domains (see, e.g., [51, 109]).

Recent theoretical results predict an IR behavior of the gluon propagator. A gluon propagator identical to zero at the momentum origin was considered in [110, 111] while another propagator was of order $1/m_g^2$ [4], where $m_g$ is the dynamical gluon mass [112]. A renormalization group analysis [113] and numerical lattice studies simulating the gluon propagator are consistent with an IR finite behavior [114]. We consider a gluon propagator:

$$\tilde{D}_{\mu\nu}^{AB}(p) = \delta^{AB}\delta_{\mu\nu}\frac{1 - \exp\left(-p^2/\Lambda^2\right)}{p^2} = \delta^{AB}\delta_{\mu\nu}\int\limits_0^{1/\Lambda^2} ds\, \mathrm{e}^{-sp^2}. \qquad (57)$$

It represents a modification of gluon propagator defined in [35] and exhibits an explicit IR-finite behavior $\tilde{D}(0) \sim 1/\Lambda^2$. For simplicity $\tilde{D}(p)$ in (57) is given in Feynman gauge.

Note, the propagators in (1) and (57) do not have any singularities in the finite $p^2$ plane in Euclidean space, thus indicating the absence of a single quark (gluon) in the asymptotic space of states. In fact, an IR parametrization is hidden in the confinement scale $\Lambda$.

The dependence of meson masses on $\hat{\alpha}_s$ and other parameters is defined by (43). Note, the polarization kernel $\lambda_{\mathcal{N}}(-p^2)$ is natively obtained real and symmetric that allows us to find a simple variational solution to this problem.

Choosing a trial Gaussian function for the ground state [35]

$$U(x) = \frac{2a}{\pi} \exp\left\{-a\Lambda^2 x^2\right\}, \quad \Lambda^4 \int d^4x \, |U(x)|^2 = 1, \quad a > 0 \qquad (58)$$

we obtain a variational form of equation (43) for meson masses as follows:

$$1 = -\hat{\alpha}_s(M_J) \cdot \lambda_J(\Lambda, M_J, m_1, m_2) =$$

$$= \frac{8\hat{\alpha}_s C_J}{3\pi^2 (m_1/\Lambda)(m_2/\Lambda)} \exp\left\{\frac{M_J^2 - (m_1 + m_2)^2}{2\Lambda^2}(\xi_1^2 + \xi_2^2)\right\} \times$$

$$\times \max_{0 < c < 2}\left[c\,(2-c)^2\right] \int\int_0^1 \frac{du\,dw}{\sqrt{(1/u - 1)(1/w - 1)}\,Q^2} \exp\left\{-\frac{M_J^2(\xi_1 - \xi_2)^2}{4\Lambda^2 Q}\right\} \times$$

$$\times \left\{\frac{2\,\rho_J}{Q} + \frac{M_J^2}{\Lambda^2}\left[\xi_1\xi_2 + \frac{(\xi_1 - \xi_2)^2}{2Q}\left(1 - \frac{\rho_J}{2Q}\right)\right] + \right.$$

$$\left. + \frac{m_1 m_2}{\Lambda^2}\left[1 + \chi_J\omega\left(\frac{m_1}{\Lambda}\right)\omega\left(\frac{m_1}{\Lambda}\right)\right]\right\}, \quad (59)$$

where $Q \doteq 1 + c(u + w)$.

Further, we exploit (59) in different ways, by solving either for $\hat{\alpha}_s$ at given masses, or for $M_J$ at known values of coupling. In doing so, we adjust the model parameters by fitting available experimental data.

Note, any physical observable must be independent of the particular scheme and mass by definition, but in (59) we obtain $\alpha_s$ depending on scaled masses $\{M_J/\Lambda, m_1/\Lambda$ and $m_2/\Lambda\}$, where $\Lambda$ is the scale of confinement. This kind of scale dependence is most pronounced in leading-order QCD and often used to test and specify uncertainties of theoretical calculations for physical observables. Conventionally, the central value of $\alpha_s(\mu)$ is determined or taken for $\mu$ equalling the typical energy of the underlying scattering reaction. There is no common agreement of how to fix the choice of scales. Particularly, in [35] we fixed the parameter $\Lambda$ by fitting light meson weak decay constants.

Below we solve (59) for different values of confinement scale. As a particular case, first we choose $\Lambda_1 = 345$ MeV.

1) We can extract intermediate values of $\alpha_s(M_V)$ in the interval 2–10 GeV from a smooth interpolation of known data from Table 1. Particularly,

$$\begin{cases} \hat{\alpha}_s(9460) = 0.1817, \\ \hat{\alpha}_s(3097) = 0.2619, \\ \hat{\alpha}_s(2112) = 0.3074, \\ \hat{\alpha}_s(2010) = 0.3138. \end{cases} \qquad (60)$$

Hereafter, masses are given in units of MeV.

Then, we derive meson mass formula and adjust the constituent quark masses $\{m_{ud}, m_s, m_c, m_b\}$ by fitting heavy meson masses $\Upsilon(9460)$, $J/\Psi(3097)$, $D_s^*(2112)$ and $D^*(2010)$:

$$\begin{cases} 1 + \hat{\alpha}_s(9460)\lambda_V(\Lambda_1, 9460, m_b, m_b) = 0, \\ 1 + \hat{\alpha}_s(3097)\lambda_V(\Lambda_1, 3097, m_c, m_c) = 0, \\ 1 + \hat{\alpha}_s(2112)\lambda_V(\Lambda_1, 2112, m_s, m_c) = 0, \\ 1 + \hat{\alpha}_s(2010)\lambda_V(\Lambda_1, 2010, m_{ud}, m_c) = 0 \end{cases} \tag{61}$$

with known masses of mesons $\Upsilon(9460)$, $J/\Psi(3097)$, $D_s^*(2112)$ and $D^*(2010)$. We fix a particular set of model parameters as follows:

$$\Lambda = \Lambda_1 = 345 \text{ MeV}, \quad m_{ud} = 192.56 \text{ MeV},$$
$$m_s = 293.45 \text{ MeV}, \quad m_c = 1447.59 \text{ MeV}, \quad m_b = 4692.51 \text{ MeV}. \tag{62}$$

Note, the masses of light constituent quarks in (62) are obtained relatively low. The reason is the singular behavior $\tilde{S}_m(\hat{p}) \sim 1/m_f$ of the quark propagator for $m_f \to 0$. On the other hand, this allows us to describe correctly light meson masses including $\pi(138)$ and $K(495)$ [35].

2) Having fixed quark masses, we solve an inverse problem, to estimate $\hat{\alpha}_s(M)$ in the region below 1 GeV by exploiting masses of mesons $\pi$, $K$, $\rho$, and $K^*$ as follows:

$$\begin{cases} \hat{\alpha}_s(138) = -\lambda_P^{-1}(\Lambda_1, 138, m_{ud}, m_{ud}) = 0.7131, \\ \hat{\alpha}_s(495) = -\lambda_P^{-1}(\Lambda_1, 495, m_{ud}, m_s) = 0.6086, \\ \hat{\alpha}_s(770) = -\lambda_V^{-1}(\Lambda_1, 770, m_{ud}, m_{ud}) = 0.4390, \\ \hat{\alpha}_s(892) = -\lambda_V^{-1}(\Lambda_1, 892, m_{ud}, m_s) = 0.4214. \end{cases} \tag{63}$$

In Fig. 11 we plot our low-energy estimates (63) in comparison with the three-loop analytic coupling, its perturbative counterpart (both normalized at the $Z$-boson mass) and the massive one-loop analytic coupling [50].

3) As an application, with particular choice of parameters (62) we calculate masses of other mesons: $D(1870)$, $D_s(1970)$, $\eta_c(2980)$, $B(5279)$, $B^*(5325)$, $B_s(5370)$, $B_c(6286)$, and $\eta_b(9389)$. Hereby, the corresponding $\alpha_s(M)$ are extracted from Fig. 9.

Our estimates of meson masses along experimental data [12] are shown in Table 2. The relative error of our estimate does not exceed 3.5 per cent in a wide range of mass.

4) By interpolating smoothly $\hat{\alpha}_s(M)$ results into intermediate-energy above 1 GeV region and taking into account correct asymptotical, we define $\hat{\alpha}_s$ on a wide interval 0.14–9.5 GeV.

5) To check the sensibility of the obtained results on the confinement scale value we recalculated steps 1)–3) for $\Lambda = 330$ MeV and $\Lambda = 360$ MeV. We
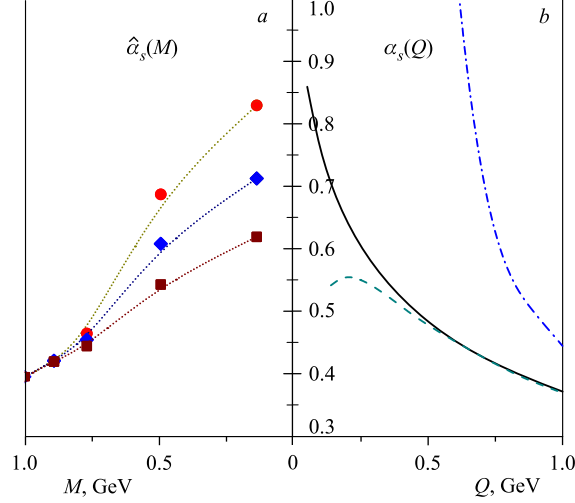
Fig. 11. Our estimates of $\hat{\alpha}_s(M)$ in the low-energy region at different values of confinement scale (in plot $a$: dots for $\Lambda = 330$ MeV, rhombs for $\Lambda = 345$ MeV, squares for $\Lambda = 360$ MeV and dotted curves are the envelope lines) compared with the three-loop analytic coupling $\alpha_s(Q)$, its perturbative counterpart and the massive one-loop analytic coupling (in plot $b$: solid, dash-dotted and dashed curves, correspondingly [50])

*Table* 2. **Masses $M$ of conventional mesons (in units of MeV) corresponding to effective coupling $\hat{\alpha}_s(M)$ determined by (59) at $\Lambda = 345$ MeV**

| $J^{PC} = 0^{-+}$ | $M_{\mathbf{P}}$ | $J^{PC} = 0^{-+}$ | $M_{\mathbf{P}}$ | $J^{PC} = 1^{--}$ | $M_{\mathbf{V}}$ | $J^{PC} = 1^{--}$ | $M_{\mathbf{V}}$ |
|---|---|---|---|---|---|---|---|
| $\pi(138)$ | 138 | $\eta_c(2980)$ | 3039 | $\rho(770)$ | 770 | $D_s^*(2112)$ | 2112 |
| $K(495)$ | 495 | $B(5279)$ | 5339 | $\omega(782)$ | 785 | $J/\Psi(3097)$ | 3097 |
| $\eta(547)$ | 547 | $B_s(5370)$ | 5439 | $K^*(892)$ | 892 | $B^*(5325)$ | 5357 |
| $D(1870)$ | 1941 | $B_c(6286)$ | 6489 | $\Phi(1019)$ | 1022 | $\Upsilon(9460)$ | 9460 |
| $D_s(1970)$ | 2039 | $\eta_b(9389)$ | 9442 | $D^*(2010)$ | 2010 | | |

revealed that the estimated meson masses shown in Table 2 do not change considerably (less than 0.5 per cent). The variation of $\hat{\alpha}_s$ under changes of $\Lambda$ is shown in Fig. 11.

6) We perform global evaluation of $\hat{\alpha}_s(M)$ at the mass scale of conventional mesons (shown in Table 2) by using formula

$$\hat{\alpha}_s(M_J) = -1/\lambda_J(M_J, \Lambda, m_1, m_2)$$

and plot the resulting curves at different $\Lambda$ in Fig. 13 in comparison with recent low- and high-energy data of $\alpha_s(Q)$ [50].

*4.2.1. IR-Finite Behavior of Effective Coupling.* The possibility that the QCD coupling constant features an IR-finite behavior has been extensively studied in recent years (e.g., [115, 116]). There are theoretical arguments in favor of a nontrivial IR-fixed point, particularly, the analytical coupling freezes at the value of $4\pi/\beta_0$ within one-loop approximation [117]. The phenomenological evidence for $\alpha_s$ finite in the IR region is much more numerous.

We note that the agreement of our estimates of $\hat{\alpha}_s(M)$ with other predictions (e.g., [85, 88]) turns out to be reasonable from 2 GeV down to the 1 GeV scale. Below this scale, different behaviors of $\alpha_s(M)$ may be expected as $M$ approaches zero.

Below we consider the IR-fixed point $\hat{\alpha}_s^0 \doteq \hat{\alpha}_s(0)$ by evaluating (59) for $M_P = 0$ and $m_1 = m_2 = m$:

$$\hat{\alpha}_s^0 = \frac{3\pi^2 m^2}{8\Lambda^2}\, e^{\mu^2} \times$$

$$\times \left\{ \max_{0<c<2} \left[c(2-c)^2\right] \int\int_0^1 \frac{du\,dw}{\sqrt{(1/u-1)(1/w-1)}(1+c(u+w))^2} \times\right.$$

$$\left. \times \left[\frac{2}{(1+c(u+w))^2} + \mu^2(1+\omega^2(\mu))\right]^{-1} \right\}^{-1}. \quad (64)$$

The dependence of $\hat{\alpha}_s^0$ on $\mu \doteq m/\Lambda$ is plotted in Fig. 12.
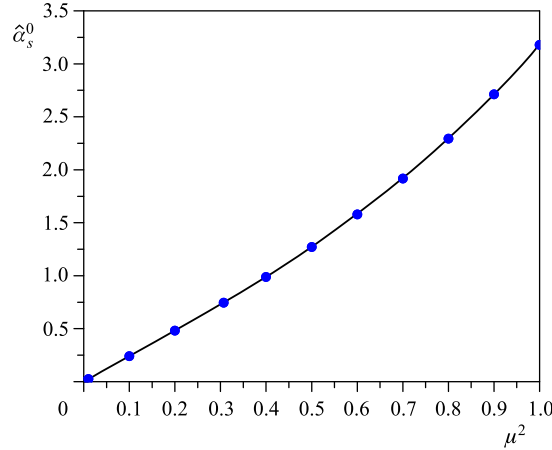


Fig. 12. The dependence of the IR-fixed point $\hat{\alpha}_s^0$ on $\mu^2 = (m/\Lambda)^2$ at $\Lambda = 345$ MeV [41]. Obviously, $\hat{\alpha}_s^0 \sim \mu^2$ for $\mu \ll 1$ and $\hat{\alpha}_s^0 \sim \exp\{\mu^2\}$ for $\mu \gg 1$

Note, a value of $\hat{\alpha}_s^0$ of order 2 or larger would be definitely out of line with many other phenomena, such as nonrelativistic potentials for charmonium [118] and analytic perturbation theory [117]. Obviously, this constraint implies an upper limit to the value of constituent quark mass: $\mu^2 < 0.8$, or $m < 0.9\Lambda$.

Since we are searching for the IR fix point, it is reasonable to choose the lightest quark mass. Particularly, for $m = m_{ud} = 192.56$ MeV and $\Lambda = 345$ MeV we obtain

$$\hat{\alpha}_s^0 = 0.757, \quad \text{or} \quad \hat{\alpha}_s^0/\pi = 0.241. \tag{65}$$

To compare our result with known data on $\alpha_s(Q)$ we exploit the integral relationships between the QCD running coupling in Euclidean and Minkowskian domains. Particularly, there exists a relation [51]:

$$\alpha_s(q^2) = q^2 \int_0^\infty \frac{ds}{(s+q^2)^2} \hat{\alpha}_s(s) \tag{66}$$

valid for the case of massless pion. By substituting $s = tq^2$ into (66) one rewrites

$$\alpha_s(q^2) = \int_0^\infty \frac{dt}{(1+t)^2} \hat{\alpha}_s(tq^2). \tag{67}$$

Then, for $q^2 \to 0$ we obtain

$$\alpha_s(0) = \hat{\alpha}_s(0) \int_0^\infty \frac{dt}{(1+t)^2} = \hat{\alpha}_s(0) \cdot 1. \tag{68}$$

Therefore, we may conclude that our result (65) is in a reasonable agreement with often quoted estimates

$$\begin{cases} \alpha_s^0/\pi \simeq 0.19{-}0.25 & [27], \\ \alpha_s^0/\pi \simeq 0.265 & [106], \\ \alpha_s^0/\pi \simeq 0.26 & [108], \\ \langle \alpha_s^0/\pi \rangle_{1\text{ GeV}} \simeq 0.2 & [17] \end{cases} \tag{69}$$

and phenomenological evidences [50, 107]. The obtained IR-fixed value of the coupling constant is moderate, it depends on the mass of constituent quark $(u, d)$, so one can insert this value into perturbative expressions to be compatible with the experimental data.

By interpolating smoothly obtained results in (65), (63), and (60) into intermediate-energy region we define $\hat{\alpha}_s$ on a wide interval 0.14–9.5 GeV. Some particular cases of the dependence of $\alpha_s$ on mass scale $M$ at different model parameters are plotted in Fig. 13.
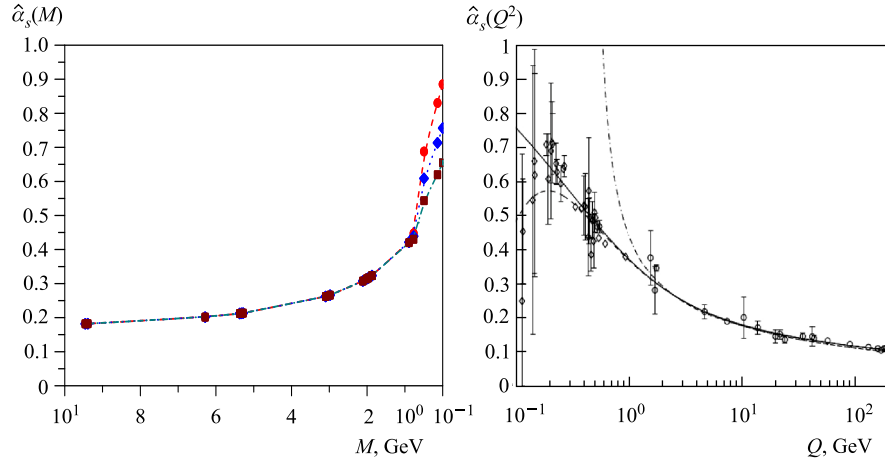
Fig. 13. Summary of estimates of $\hat{\alpha}_s(M)$ in the interval from 0 to 10 GeV at different values of confinement scale: $\Lambda = 330$ MeV (dots), $\Lambda = 345$ MeV (rhombs) and $\Lambda = 360$ MeV (squares) compared with $\alpha_s(Q)$ defined in low- (diamonds) and high-energy (circles) experiments. Also shown are the three-loop analytic coupling (solid curve), its perturbative counterpart (dash-dotted curve) both normalized at the $Z$-boson mass and the massive one-loop analytic coupling (dashed curve) (for details see in [50])

It is important to stress that we do not aim to obtain the behavior of the coupling constant at all scales. At moderate $M^2 = -p^2$ we obtain $\alpha_s$ in coincidence with the QCD predictions. However, at large mass scale (above 10 GeV) $\hat{\alpha}_s$ decreases much faster than expected by QCD prediction. The reason is the use of confined propagators in the form of entire functions (1) and (57). Then, the convolution of entire functions leads to a rapid decreasing (or, a rapid growth in Minkowski space) of physical matrix elements once the hadron masses and energies of the reaction have been fixed. Consequently, the numerical results become sensitive to changes of model parameters at large masses and energies.

To conclude, we provide an estimate of QCD effective charge in the low energy region (below 1 GeV) by exploiting the conventional meson spectrum within a relativistic quantum-field model based on analytic (or, infrared) confinement. The new results obtained in the previous section are summarized in Figs. 11, 12, 13 and Table 2.

Despite its pure model origin, used approximations and questionings about the very definition of the coupling in the IR region, our approach demonstrates a new, independent and specific IR-finite behavior of QCD coupling and we extract a particular IR-fixed point at $\hat{\alpha}_s(0) \simeq 0.757$ for confinement scale $\Lambda = 345$ MeV. As an application, we performed estimates on intermediate and heavy meson masses and the result was in reasonable agreement with experimental data. Our

estimates may be improved further by using iterative schemes, but the aim is to obtain a qualitative understanding of QCD effective coupling in the IR region.

Note, further improvements of measurements of $\alpha_s$ will be difficult while it is unlikely that QCD perturbation theory will considerably improve existing predictions. Therefore, further developments of theoretical predictions within nonperturbative methods and reapplication of improved models may have successes in this field.


## CONCLUSION


In the present review, we demonstrate that global properties of the low-energy phenomena such as QCD running coupling, the lowest-state glueball, the weak decay constants of light mesons, and the conventional meson spectrum may be explained reasonably in the framework of a simple relativistic quantum-field model of quark-gluon interaction based on analytic (or, infrared) confinement.

In doing so, first we considered simple scalar («toy») models of Yukawa-type interaction which explained qualitatively the experimental evidences: the constituent particles are confined, their final bound-states are stable, massless «gluons» constitute the «glueballs», and the Regge trajectories of «meson» orbital excitations are asymptotically linear.

Then, we provided a new, independent, and analytic estimate of the lowest glueball mass, and we found it at 1661 MeV within a relativistic quantum-field model based on AC. The conventional mesons and the weak decay constants are described to extend the consideration. For the spectra of two-gluon and two-quark bound states we solve the ladder BSE. By using a minimal set of model parameters (the quark masses, the coupling constant, and the confinement scale) we obtain numerical results which are in reasonable agreement with experimental evidence in the wide range of energy scale.

Finally, we estimate the QCD effective charge $\alpha_s$ in the low-energy region. Despite its pure model origin, used approximations and questionings about the very definition of the coupling in the IR region, our approach demonstrates a new, independent and specific IR-finite behavior of QCD coupling and we extract a particular IR-fixed point at $\hat{\alpha}_s(0) \simeq 0.757$ for confinement scale $\Lambda = 345$ MeV. As an application, we estimate masses of some intermediate and heavy mesons and obtain results in reasonable agreement with recent experimental data.

The suggested models in their simple forms are far from real QCD but we can conclude that the AC conception combined with BSE method serves a reasonable framework to describe simultaneously different sectors in low-energy particle physics and may provide us with a rather satisfactory correlated understanding of low and intermediate energy phenomena in a wide range from few hundreds MeV

to few GeV. Our guess about the symmetry structure of the quark–gluon interaction in the confinement region has been tested and the use of simple forms of propagators has resulted in quantitatively reasonable estimates in different sectors of the low-energy particle physics. The consideration can be extended to other problems in hadron physics.

## APPENDIX A

Consider the kernel

$$K = K(x, y) = e^{-ax^2 + 2bxy - ay^2}, \quad a > b \tag{70}$$

with

$$\text{Tr } K = \int dy \, K(y, y) = \int dy \, e^{-2(a-b)y^2} = \frac{\pi^2}{4(a-b)^2} < \infty.$$

The eigenvalues with quantum numbers $Q = \{nl\{\mu\}\} = \{nl\{\mu_1, \ldots, \mu_l\}\}$ and eigenfunctions of the problem

$$\int dy \, K(x, y) \, U_Q(y) = \kappa_Q U_Q(x)$$

can be solved explicitly. The eigenvalues are

$$\kappa_Q = \kappa_{nl} = \kappa_0 \left( \frac{b}{a + \sqrt{a^2 - b^2}} \right)^{2n+l}, \quad \kappa_0 = \frac{\pi^2}{(a + \sqrt{a^2 - b^2})^2}. \tag{71}$$

The eigenfunctions are

$$U_Q = U_{nl\{\mu\}}(y) = N_{nl} \, T_{l\{\mu\}}(y) L_n^{(l+1)} \left(2\beta y^2\right) e^{-\beta y^2}. \tag{72}$$

Here $L_n^{(l+1)}(x)$ are the Laguerre polynomials and

$$\beta = \sqrt{a^2 - b^2}, \quad N_{nl} = \frac{\sqrt{2^l(l+1)}}{\pi} (2\beta)^{1 + \frac{l}{2}} \sqrt{\frac{\Gamma(n+1)}{\Gamma(n+l+2)}}.$$

The functions

$$T_{l\{\mu\}}(y) = T_{l\{\mu\}}(n_y)|y|^l, \quad n_y = \frac{y}{|y|}, \quad |y| = \sqrt{y^2}$$

satisfy the conditions

$$T_{l\{\mu_1\mu_2,\ldots,\mu_l\}}(n) = T_{l\{\mu_2\mu_1,\ldots,\mu_l\}}(n), \quad T_{l\{\mu\mu\mu_3,\ldots,\mu_l\}}(n) = 0,$$

$$\sum_{\{\mu\}} T_{l\{\mu\}}(n_1)T_{l\{\mu\}}(n_2) = \frac{1}{2^l}C_l^1((n_1n_2)), \quad C_l^1(1) = l+1,$$

where $C_l^1(t)$ are the Gegenbauer polynomials and

$$\int dn\, T_{l\{\mu\}}(n)\, T_{l'\{\mu'\}}(n) = \delta_{ll'}\delta_{\{\mu\}\{\mu'\}}\frac{2\pi^2}{2^l(l+1)}.$$

Besides, the following relation takes place

$$\int d^4y\, T_{l\{\mu\}}(y)F(y^2)\,\mathrm{e}^{-iky} = \left(\frac{-i}{2\pi}\right)^l T_{l\{\mu\}}(k)J(k^2),$$

$$J(k^2) = \int dY\,\mathrm{e}^{-iKY}F(Y^2), \quad K,Y \in \mathbf{R}^{4+2l}, \quad k^2 = K^2. \tag{73}$$

## APPENDIX B

Let us consider the variational problem (25) for the lowest state ($n = l = 0$) in the deconfinement limit $\Lambda \to 0$. We have

$$4\alpha_0\left(\frac{m}{\Lambda}\right)^2 \max_{0<c<1} \left\{ c(1-c)\int\int_0^1 dt\,ds\, \exp\left[-\left(\frac{m^2}{\Lambda^2} - \frac{M_0^2}{4\Lambda^2}\right)(t+s)\right] \times \right.$$

$$\left. \times \int\int_0^1 du\,dv\, \frac{\exp\left\{-\dfrac{M_0^2}{4\Lambda^2}\dfrac{(t-s)^2}{t+s+2c(u+v)}\right\}}{[t+s+2c(u+v)]^2} \right\} = 1. \tag{74}$$

Here $M_0$ is the mass of the lowest bound state and the effective coupling constant is supposed small

$$\alpha_0 = \left(\frac{g}{4\pi m}\right)^2 \ll 1.$$

Going to the new variables

$$t = \frac{\Lambda^2}{2m^2}(x+y), \quad s = \frac{\Lambda^2}{2m^2}(x-y), \quad c = \frac{\Lambda^2}{m^2}\xi$$

one can rewrite (74) in the limit $\Lambda \to 0$ (which exists if $M_0 < 2m$) as follows:

$$2\alpha_0 \max_{\xi} \left\{ \xi \int_0^\infty dx \exp\left[ -\left(1 - \frac{M_0^2}{4m^2}\right) x \right] \int_0^1 \int \frac{du\, dv}{[x + 2\xi(u+v)]^2} \int_{-x}^x dy \times \right.$$

$$\left. \times \exp\left[ -\frac{M_0^2}{4m^2} \frac{y^2}{x + 2\xi(u+v)} \right] \right\} = 1.$$

If $\alpha_0 \ll 1$, then $1 - M_0/2m \ll 1$ and the main contribution to the integral over $dx$ comes from large $x$, so that the inner integral over $dy$ can be explicitly taken on the extended interval $\{-\infty, \infty\}$. Thus, we get

$$\frac{4m\alpha_0}{M_0} \sqrt{\frac{\pi}{1 - M_0^2/4m^2}} C = 1,$$

$$(75)$$

$$C = \max_{0 < \xi < \infty} \left\{ \xi \int_0^\infty dx\, e^{-x} \int_0^1 \int \frac{du\, dv}{[x + 2\xi(u+v)]^{3/2}} \right\} = 0.31923\ldots$$

By solving (75) one obtains the mass of the lowest two-particle bound state in the deconfinement limit $\Lambda \to 0$ as follows

$$M_0 = 2m - \frac{\alpha_0^2}{2} tm\, K + O(\alpha_0^4), \quad K = 2\pi C^2 = 0.6403\ldots$$

## REFERENCES

1. *Weinberg S.* The Quantum Theory of Fields. Cambridge Univ. Press, 1995.

2. *Miransky V. A.* Dynamical Symmetry Breaking in Quantum Field Theories. World Sci., 1993.

3. *Fischer C. S., Alkofer R.* hep-ph/0301094.

4. *Leutwyler H.* // Phys. Lett. B. 1980. V. 96. P. 154; Nucl. Phys. B. 1981. V. 179. P. 129.

5. *Sting M.* // Phys. Rev. D. 1984. V. 29. P. 2105.

6. *Kraan T. C., van Baal P.* // Nucl. Phys. B. 1998. V. 533. P. 627.

7. *Alkofer R., Greensite J.* // J. Phys. G. 2007. V. 34. P. 3.

8. *Lenz F., Negele J. W., Thies M.* // Phys. Rev. D. 2004. V. 69. P. 074009.

9. *Elizalde E., Soto J.* // Nucl. Phys. B. 1985. V. 260. P. 136.

10. *Burdanov J. V. et al.* // Phys. Rev. D. 1996. V. 54. P. 4483.

11. *Baldicchi M., Prosperi G. M.* hep-ph/0310213.

12. *Amsler C. et al.* // Phys. Lett. B. 2008. V. 667. P. 1.

13. *Gasser J., Leutwyler H.* // Ann. Phys. 1984. V. 158. P. 142; Nucl. Phys. B. 1985. V. 250. P. 465.

14. *Shifman M. A., Vainshtein A. I., Zakharov V. I.* // Nucl. Phys. B. 1979. V. 147. P. 385.

15. *Neubert M.* // Phys. Rep. 1994. V. 245. P. 259.

16. *Davies C. T. H. et al. (HPQCD Collab.)* // Phys. Rev. D. 2008. V. 78. P. 114507.

17. *Dokshitzer Yu. L., Marchesini G., Webber B. R.* // Nucl. Phys. B. 1996. V. 469. P. 93; *Dokshitzer Yu. L., Khoze V. A., Troyan S. I.* // Phys. Rev. D. 1996. V. 53. P. 89.

18. *Corcella G. et al.* // JHEP. 2001. V. 0101. P. 010.

19. *Gupta R.* hep-lat/9807028.

20. *Roberts C. D.* nucl-th/0802.0217; *Roberts C. D., Schmidt S. M.* // Prog. Part. Nucl. Phys. 2000. V. 45. P. 1.

21. *Salpeter E. E., Bethe H. A.* // Phys. Rev. 1951. V. 84. P. 1232.

22. *Roberts C. D., Williams A. G.* // Prog. Part. Nucl. Phys. 1994. V. 33. P. 477.

23. *Tang A., Norbury J. W.* // Phys. Rev. D. 2000. V. 62. P. 016006.

24. *Regge T.* // Nuovo Cim. 1959. V. 14. P. 951; 1960. V. 18. P. 947.

25. *Chew G. F., Frautschi S. C.* // Phys. Rev. Lett. 1962. V. 8. P. 41.

26. *Collins P. D. B.* An Introduction to Regge Theory. High Energy Physics. Cambridge Univ. Press, 1977.

27. *Godfrey S., Isgur N.* // Phys. Rev. D. 1985. V. 32. P. 189; *Barnes T., Close F. E., Monaghan S.* // Nucl. Phys. B. 1983. V. 198. P. 380.

28. *Leinweber D. B. et al.* // Phys. Rev. D. 1999. V. 60. P. 094507.

29. *Cucchieri A., Zwanziger D.* hep-ph/0012024.

30. *Maung K. M., Kahana D. E., Norbury J. W.* // Phys. Rev. D. 1993. V. 47. P. 1182; V. 48. P. 3408.

31. *Burdanov Ya. V., Efimov G. V.* // Phys. Rev. D. 2001. V. 64. P. 014001.

32. *Efimov G. V., Ivanov M. A.* The Quark Confinement Model of Hadrons. IOP Publ. Ltd, 1993.

33. *Ahlig A. et al.* // Phys. Rev. D. 2001. V. 64. P. 014004.

34. *Ganbold G.* // PoS. 2008. V. Confinement 8. P. 085.

35. *Ganbold G.* // Phys. Rev. D. 2009. V. 79. P. 034034.

36. *Ebert D., Feldmann T., Reinhardt H.* // Phys. Lett. B. 1996. V. 388. P. 154.

37. *Volkov M. K., Yudichev V. L.* // Phys. At. Nucl. 2000. V. 63. P. 464.

38. *Aguilar A. C. et al.* // Phys. Rev. D. 2009. V. 80. P. 085018.

39. *Shirkov D. V.* // Theor. Math. Phys. 2002. V. 132. P. 1309.

40.  *Feldman T. //* Intern. J. Mod. Phys. A. 2000. V. 15. P. 159.

41.  *Ganbold G. //* Phys. Rev. D. 2010. V. 81. P. 094008.

42.  *Efimov G. V., Ganbold G.* hep-ph/0103101.

43.  *Ganbold G.* Hadron Spectrum and Analytic Confinement // Proc. of the 6th Workshop on Nonperturbative QCD. 2001.

44.  *Efimov G. V., Ganbold G. //* Phys. Rev. D. 2002. V. 65. P. 054012.

45.  *Ganbold G. //* AIP Conf. Proc. 2004. V. 717. P. 285; 2005. V. 796. P. 127.

46.  *Ganbold G.* hep-ph/0512287.

47.  *Ganbold G.* hep-ph/0610399.

48.  *Ganbold G.* hep-ph/0611277.

49.  *Ganbold G. //* EConf. 2007. C070910. P. 228.

50.  *Baldicchi M. et al. //* Phys. Rev. D. 2008. V. 77. P. 034013.

51.  *Nesterenko A. V. //* Intern. J. M. Phys. A. 2003. V. 18. P. 5475.

52.  *Kaczmarek O., Zantow F. //* Phys. Rev. D. 2005. V. 71. P. 114510.

53.  *Fischer C. S., Zwanziger D. //* Ibid. V. 72. P. 054005.

54.  *Bernard C. et al. (MILC Collab.) //* PoS. 2007. LAT2007. P. 090.

55.  *Beane S. R. et al. (NPQCD Collab.) //* Phys. Rev. D. 2007. V. 75. P. 094501.

56.  *Follana E. et al. (HPQCD Collab.).* hep-lat/0706.1726.

57.  *Bernard C. et al. //* PoS. 2005. LAT2005. P. 025.

58.  *Klempt E., Zaitsev A. //* Phys. Rep. 2007. V. 454. P. 1.

59.  *Amsler C., Tornqvist N. A. //* Phys. Rep. 2004. V. 389. P. 61.

60.  *Bugg D. V. //* Ibid. V. 397. P. 257.

61.  *Yao W. M. et al. //* J. Phys. G. 2006. V. 33. P. 1.

62.  *Bugg D. V., Peardon M. J., Zou B. S. //* Phys. Lett. B. 2000. V. 486. P. 49.

63.  *Sexton J., Vaccarino A., Weingarten D. //* Phys. Rev. Lett. 1995. V. 75. P. 4563.

64.  *Chanowitz M. S. //* Phys. Rev. Lett. 2007. V. 98. P. 149104.

65.  *Ablikim M. et al. (BES Collab.) //* Phys. Rev. Lett. 2006. V. 96. P. 162002.

66.  *Narison S. //* Nucl. Phys. B. 1998. V. 509. P. 312; Nucl. Phys. A. 2000. V. 675. P. 54.

67.  *Szczepaniak A. P., Swanson E. S. //* Phys. Lett. B. 2003. V. 577. P. 61.

68.  *Cornwall J. M., Soni A. //* Phys. Lett. B. 1983. V. 120. P. 431.

69.  *Brau F., Semay C., Silvestre-Brac B. //* Phys. Rev. D. 2004. V. 70. P. 014017.

70.  *Kaidalov A. B., Simonov Yu. A. //* Phys. Lett. B. 2006. V. 636. P. 101.

71.  *Mathieu V., Semay C., Silvestre-Brac B. //* Phys. Rev. D. 2006. V. 74. P. 054002.

72.  *Yamada K. et al. //* Prog. Theor. Phys. 1997. V. 97. P. 813.

73. *Soloviev L. D.* // Theor. Math. Phys. 2001. V. 126. P. 203.

74. *Mathieu V., Semay C., Brau F.* // Eur. Phys. J. A. 2006. V. 27. P. 225.

75. *Morningstar C. J., Peardon M.* // Phys. Rev. D. 1999. V. 60. P. 034509.

76. *Meyer H. B., Teper M. J.* // Phys. Lett. B. 2005. V. 605. P. 344.

77. *Ochs W.* hep-ph/0609207.

78. *Vaccarino A., Weingarten D.* // Phys. Rev. D. 1999. V. 60. P. 114501.

79. *Chen Y. et al.* // Phys. Rev. D. 2006. V. 73. P. 014516.

80. *Mathieu V., Buisseret F., Semay C.* // Phys. Rev. D. 2008. V. 77. P. 114022.

81. *Bali G. S.* hep-ph/0110254.

82. *Ishii N., Suganuma H., Matsufuru H.* hep-lat/0106004.

83. *Shifman M. A.* Preprint University Minnesota. TRI-MINN-98/10-T 1998; UMN-TH-1622-98. 1998.

84. *Chekanov S. et al.* // Phys. Lett. B. 2003. V. 560. P. 7.

85. *Bethke S.* // J. Phys. G. 2000. V. 26. P. 27.

86. *Bethke S.* // Eur. Phys. J. C. 2009. V. 64. P. 689.

87. *Bethke S.* // Prog. Part. Nucl. Phys. 2007. V. 58. P. 351.

88. *Prosperi G. M., Raciti M., Simolo C.* // Ibid. V. 58. P. 387.

89. *Nesterenko A. V., Papavassiliou J.* // Phys. Rev. D. 2005. V. 71. P. 016009;
    *Beneke M., Jamin M.* // JHEP. 2008. V. 0809. P. 044.

90. *Narison S.* // Phys. Lett. B. 2009. V. 673. P. 30.

91. *Davier M. et al.* // Eur. Phys. J. C. 2008. V. 56. P. 305.

92. *Davies C. et al.* // Nucl. Phys. Proc. Suppl. 2003. V. 119. P. 595.

93. *Penin A., Pivovarov A. A.* // Phys. Lett. B. 1998. V. 435. P. 413.

94. *Movilla Fernandez P. A.* hep-ex/0205014. 2002.

95. *Mattingly A. C., Stevenson P. M.* // Phys. Rev. D. 1994. V. 49. P. 437.

96. *Aguilar A. C., Mihara A., Natale A. A.* // Phys. Rev. D. 2002. V. 65. P. 054011.

97. *Bloch J. C. R.* // Ibid. V. 66. P. 034032.

98. *Zwanziger D.* // Ibid. V. 65. P. 094039.

99. *Capitani S. et al.* // Nucl. Phys. B. 1999. V. 544. P. 669.

100. *Sternbeck A. et al.* // PoS. 2007. LAT2007. P. 256.

101. *Boucaud P. et al.* // Phys. Rev. D. 2004. V. 70. P. 114503.

102. *Buchmuller W., Grunberg G., Tye S.-H. H.* // Phys. Rev. Lett. 1980. V. 45. P. 103; 587.

103. *Peter M.* // Phys. Rev. Lett. 1997. V. 78. P. 602;
     *Schroder Y.* // Phys. Lett. B. 1999. V. 447. P. 321.

104. *Brambilla N. et al.* // Phys. Rev. D. 1999. V. 60. P. 091502; Nucl. Phys. B. 2000. V. 566. P. 275.

105. *Baker M. et al.* // Phys. Rev. D. 1996. V. 54. P. 2829.

106. *Zhang T., Koniuk R.* // Phys. Lett. B. 1991. V. 261. P. 311; *Ji C. R., Amiri F.* // Phys. Rev. D. 1990. V. 42. P. 3764.

107. *Baldicchi M., Prosperi G. M.* // AIP Conf. Proc. 2005. V. 756. P. 152; *Baldicchi M., Prosperi G. M.* // Phys. Rev. D. 2002. V. 66. P. 074008.

108. *Halzen F., Krein G. I., Natale A. A.* // Phys. Rev. D. 1993. V. 47. P. 295.

109. *Milton K. A., Solovtsov I. L.* // Phys. Rev. D. 1997. V. 55. P. 5295; 1999. V. 59. P. 107701.

110. *Fischer C. S., Alkofer R., Reinhardt H.* // Phys. Rev. D. 2002. V. 65. P. 094008; *Fischer C. S., Alkofer R.* // Phys. Lett. B. 2002. V. 536. P. 177.

111. *Lerche C., von Smekal L.* // Phys. Rev. D. 2002. V. 65. P. 125006.

112. *Alles B. et al.* // Nucl. Phys. B. 1997. V. 502. P. 325.

113. *Gies H.* // Phys. Rev. D. 2002. V. 66. P. 025006.

114. *Langfeld K., Reinhardt H., Gattnar J.* // Nucl. Phys. B. 2002. V. 621. P. 131.

115. *Brodsky S. J., de Teramond G. F.* // Phys. Lett. B. 2004. V. 582. P. 211.

116. *Aguilar A. C., Mihara A., Natale A. A.* // Intern. J. Mod. Phys. A. 2004. V. 19. P. 249.

117. *Shirkov D. V., Solovtsov I. L.* // Phys. Rev. Lett. 1997. V. 79. P. 1209; *Shirkov D. V.* // Theor. Math. Phys. 2003. V. 136. P. 893.

118. *Badalian A. M., Bakker B. L. G.* // Phys. Rev. D. 2000. V. 62. P. 094031.